

Discriminating fluvial fans and deltas: Channel network morphometrics reflect distinct formative processes

Luke Gezovich^{1*}, Piret Plink-Björklund¹, Jack Henry^{1,2}

¹ Colorado School of Mines, Geology & Geologic Engineering, 1500 Illinois Street, Golden, CO, 80401

² Rice University, Earth, Environmental and Planetary Sciences, 6100 Main St., Houston, TX, 77005-1827

Correspondence to: Luke Gezovich (lukegezovich@mines.edu)

Abstract

Recent recognition of a new type of fluvial system – fluvial fans – introduces a fan-shaped channel network that appears similar to that of river-dominated deltas. Deltas form where rivers enter lakes and oceans, while fluvial fans are terrestrial landforms. However, fluvial fans can reach the shorelines of oceans or lakes, and in such cases the distinction between fluvial fan and river-dominated delta channel networks becomes ambiguous. We currently lack fundamental understanding of these two landforms’ morphometric differences, despite their high socioeconomic significance, vulnerability to natural hazards, and key differences in how these landforms respond to global climate change and urbanization. Here we review the relevant conceptual differences in delta and fluvial fan network morphodynamics, propose a set of quantitative morphometric criteria to distinguish fluvial fan and delta channel networks, and test these criteria on 40 deltas and 40 fluvial fans from across the world. This initial attempt to contrast and distinguish deltas and fluvial fans based on their channel network morphometrics demonstrates that quantifying channel network angles (mean of 73.8° for deltas and 55.0° for fluvial fans) and trends in normalized channel widths and lengths provide efficient criteria, but some ambiguities remain that need to be resolved in future work. This research advances our mechanistic understanding of fluvial fan and delta channel networks and the recognition of modern and ancient landforms on Earth and other planetary bodies, such as Mars and Saturn’s moon Titan.

Plain Language Summary

Fluvial fans are a newly recognized type of river system that look like river deltas, especially when they reach lakes or oceans. This study explores how to tell them apart by measuring the size and layout of channels in these fan-shaped landforms. Understanding these differences helps to predict how these landforms respond to climate change and urbanization, and to identify them on Mars and other planetary bodies.

37 1. Introduction

38 River deltas are depositional landforms that form where rivers enter lakes or oceans. They are
39 home to over half a billion people, host abundant and biodiverse ecosystems, and function as both
40 economic and agricultural hubs (Saito et al., 2007; Tejedor et al., 2015). The form and function of deltas
41 is intimately linked to the evolving structure of their channel networks that determine how deltas
42 distribute sediment and nutrients (Passalacqua, 2017; Pearson et al., 2020; Tejedor et al., 2017). Delta
43 channel network morphology results from an intricate balance between sediment erosion and deposition
44 from river, tide, and wave energy fluxes. River fluxes create distributary channels and islands, tides
45 roughen the shoreline and widen the channels, and waves smooth the shoreline and decrease the number
46 of distributary channels (Broaddus et al., 2022; Galloway, 1975; Nienhuis et al., 2015, 2018; Paniagua-
47 Arroyave & Nienhuis, 2024; Vulis et al., 2023). Deltas dominated by river energy fluxes (river-dominated
48 deltas) (Broaddus et al., 2022; Galloway, 1975; Nienhuis et al., 2015, 2018; Paniagua-Arroyave &
49 Nienhuis, 2024; Vulis et al., 2023) characteristically form fan-shaped landforms with complex
50 distributary channel networks (Fig. 1). In these deltas, channel network topology is defined by mouth bar
51 deposition and consequent distributary channel bifurcation (Bates, 1953; Edmonds & Slingerland, 2007;
52 Wright, 1977). To specifically refer to these deltaic processes, we define “bifurcations” as a process
53 related to mouth bar deposition and consequent channel branching.

54 Fluvial fans are another type of fan-shaped landform with channel networks that share
55 morphological similarities with the river-dominated delta channel networks (Fig. 2). Fluvial fans are a
56 relatively newly acknowledged type of fluvial landform (Ventra & Clarke, 2018; Weissman et al., 2010),
57 which forms via river avulsions or “channel jumps” across low-gradient floodplains (Chakraborty et al.,
58 2010; Martin & Edmonds, 2023; North & Warwick, 2007). Rivers have been traditionally regarded as
59 sediment transfer or bypass zones in source-to-sink systems (Allen, 2008; Fielding et al., 2012), whereas
60 fluvial fans are net depositional and build significant stratigraphic thicknesses (Chakraborty et al., 2010;
61 Moscariello, 2018; Weissmann et al., 2015). Fluvial fans are also called “wet” fluvial-dominated alluvial
62 fans (Schumm, 1977), megafans (Singh et al., 1993), or distributive fluvial systems (DFS) (Weissman et
63 al., 2010). Fluvial fans are distinct landforms from alluvial fans – which form by a combination of
64 gravitational and streamflow processes, feature steep gradients (typically 2–12°), and have a relatively
65 small radius typically less than 10 km (Blair & McPherson, 1994; Moscariello, 2018). Fluvial fans form
66 some of the largest terrestrial landforms on Earth (10^3 – 10^5 km² in surface area) (Horton & Decelles, 2001;
67 Leier et al., 2005) and have low gradients (typically 0.03–0.001°) (Brooke et al., 2022). Fluvial fans are
68 abundant across Earth, and they form in diverse climatic and tectonic settings (Hartley et al., 2010; Ventra
69 & Clarke, 2018; Weissmann et al., 2010).

70 Like deltas, fluvial fans are home to hundreds of millions of people, and these highly dynamic
71 landforms are critical for their livelihood – supporting agriculture, fisheries, and freshwater access. For
72 example, the Kosi fluvial fan experiences catastrophic river floods that lead to large numbers of casualties
73 and displaced populations (Sinha, 2009; Syvitski & Brakenridge, 2013). While fluvial fans are terrestrial
74 landforms, they can reach the shorelines of oceans (Fig. 2b) or lakes (Figs. 2a, 2d and 2i). In such cases
75 the distinction between fluvial fan and river-dominated delta channel networks becomes ambiguous,
76 while wave- and tide-dominated deltas have distinctly recognizable morphologies (Broaddus et al., 2022;
77 Galloway, 1975; Nienhuis et al., 2015; 2018; Paniagua-Arroyave & Nienhuis, 2024; Vulis et al., 2023).
78 We currently lack quantitative morphometric criteria for distinguishing river-dominated delta and fluvial
79 fan channel networks, despite their socioeconomic significance, key differences in their natural hazard
80 vulnerabilities, and in how they respond to global change. Deltas are global change hotspots highly
81 vulnerable to urbanization and climate change, which can aggravate coastal hazards and cause sea level
82 rise (Giosan et al., 2014; Syvitski et al., 2009), and reduce sediment supply due to river damming and
83 artificial levees, causing the drowning of deltas (Blum & Roberts, 2009; Giosan et al., 2014; Nienhuis et
84 al., 2020; Paola et al., 2011; Syvitski et al., 2009).

85 Numerous fan-shaped landforms with channel networks have also been identified on other planetary
86 bodies such as Mars (Malin & Edgett, 2015; Ori et al., 2000; Wood, 2006) and Saturn’s moon Titan
87 (Radebaugh et al., 2018; Wall et al., 2010; Witek & Czechowski, 2015). Deltas on planetary bodies are
88 important indicators of paleo-shorelines and have been utilized to reconstruct the shorelines and water
89 levels of ancient lakes and oceans on Mars (Di Achille & Hynek, 2010). However, Martian paleo-ocean
90 shoreline reconstructions have so far yielded mixed results (De Toffoli et al., 2021). This discrepancy
91 could perhaps arise because shoreline-bound deltas have not been effectively distinguished from fluvial
92 fans on Mars, which may form thousands of kilometers inland from shorelines (Bramble et al., 2019;
93 Limaye et al., 2023; Tebolt & Goudge, 2022). Deltas also offer attractive targets for mission sites in
94 search of life due to their habitability and high biosignature preservation potential, as exemplified by the
95 selection of Jezero Crater for NASA’s *Perseverance* rover, *Ingenuity* helicopter, and future Mars Sample
96 Return mission (Farley et al., 2020). Distinguishing deltaic and fluvial fan paleo-channel networks on
97 other planetary bodies is even more ambiguous, especially if the lakes and oceans are no longer present.

98 Over time, the accumulation of biogenic and sedimentary materials distributed via channel networks
99 contributes to the construction of stratigraphy. Fluvial fans and deltas are net depositional systems, as
100 both are characterized by spatially diminishing water surface slopes that reduce sediment transport
101 capacity, thereby producing spatiotemporal convergence and deposition of sediment (Ganti et al., 2014).
102 Consequently, in addition to their socioeconomic significance, both landforms significantly contribute to
103 the stratigraphic record, and their deposits can be used to decipher past environmental conditions. High

104 deposition rates in fluvial fans and deltas promote the preservation of environmental change signals in the
105 sedimentary record (Trampusch & Hajek, 2017). Similar to modern river-dominated deltas and fluvial
106 fans, we lack morphometric criteria to distinguish these two fan-shaped channel networks in the
107 sedimentary record, such as in seismic datasets.

108 This study is motivated by developing quantitative morphometric distinction criteria for fluvial fan
109 and river-dominated delta channel networks. Prior work has established quantitative morphological
110 criteria for describing deltaic channel networks and linked these characteristics to theory (Chen et al.,
111 2021; Coffey & Shaw, 2017; Edmonds et al., 2011; Edmonds & Slingerland, 2007; Fagherazzi et al.,
112 2015; Ke et al., 2019; Passalacqua, 2017; Pearson et al., 2020; Tejedor et al., 2015, 2017). However, there
113 are no existing quantitative criteria to characterize fluvial fan channel networks or to differentiate the two
114 landforms. To develop such criteria, we review the relevant conceptual differences in delta and fluvial fan
115 network morphodynamics, propose quantitative morphometric criteria to distinguish fluvial fan and delta
116 channel networks, and test these criteria on 40 deltas and 40 fluvial fans (Supplementary Data) from
117 across the globe (Fig. 3). We test the robustness of the approach by analyzing differences in channel
118 network morphometrics concerning the size and gradient of the systems, hydroclimate conditions, lake
119 versus ocean terminations and tide versus wave influences in deltas, and channel morphology in fluvial
120 fans. We assess how effectively the proposed methods distinguish fluvial fans from river-dominated
121 deltas and examine why this distinction matters under global change. This work serves to improve our
122 mechanistic understanding of fluvial fan and delta evolution, and their accurate recognition on Earth,
123 other planetary bodies, and in the sedimentary record.

124 **2. Delta and Fluvial Fan Channel Network Morphodynamics**

125 The nature of channel networks is dependent on distinct morphodynamic processes responsible for
126 their formation (Edmonds & Slingerland, 2007; Fagherazzi et al., 2015; Tejedor et al., 2015). Below we
127 analyze differences in delta and fluvial fan morphodynamics and review existing morphometric criteria
128 for quantifying deltaic distributary channel networks. Our review is not comprehensive; rather, it focuses
129 on the specific processes that govern the formation of the morphometric characteristics that we can then
130 use for distinction of these two landforms, namely channel network angles, and downstream changes in
131 channel widths and lengths. There are other important characteristics of deltaic channel networks, linked
132 to water and sediment discharge distribution, entropy, and connectivity (Chen et al., 2021; Ke et al., 2019;
133 Passalacqua, 2017; Pearson et al., 2020; Tejedor et al., 2015, 2017). These aspects are not considered in
134 this review, because they are outside the scope of this study that seeks to distinguish deltaic and fluvial
135 fan channel networks using easily applicable morphometric criteria that can be used for both deltaic and
136 fluvial fan networks.

137 We use the terms bifurcation and avulsion as *processes* rather than a geomorphological feature of
138 channel splitting. *Bifurcation* is the process of channel splitting driven by mouth bar formation (Edmonds
139 & Slingerland, 2007). *Avulsions* are channel “jumps”, where a channel changes its course due to channel
140 superelevation or a more favorable (steeper) gradient at channel flanks (Gearon et al., 2024; Jones &
141 Schumm, 1999; Slingerland & Smith, 2004). Partial avulsions split channels; however, the process is
142 distinct from *bifurcation* around a mouth bar.

143 **2.1 River Deltas**

144 Deltas (Fig. 1) form only where a river enters a standing body of water. Here, the transport capacity
145 of the turbulent jet decreases, and the “parent” stream jet flow experiences both lateral and bed friction,
146 causing the flow to decelerate and rapidly expand laterally (Bates, 1953; Edmonds & Slingerland, 2007;
147 Jerolmack & Swenson, 2007; Wright, 1977). As a result, the transport capacity of the turbulent jet
148 decreases and sediment is deposited as a mouth bar basinward of the river mouth (Edmonds &
149 Slingerland, 2007). The process of mouth bar deposition and growth eventually leads to the bifurcation, or
150 downstream branching of a single (parent) channel into two daughter channels (Axelsson, 1967; Coffey &
151 Shaw, 2017; Edmonds & Slingerland, 2007) (Fig. 4a). These daughter channels are separated by an island
152 or shallow bay where sediment transport is significantly reduced or nonexistent, and flow is
153 unchanneled (Coffey & Shaw, 2017). Mouth bar deposition and resultant channel bifurcation repeat
154 multiple times, leading to the seaward advancement of the shoreline and the construction of a delta
155 distributary channel network (Edmonds & Slingerland, 2007; Olariu & Bhattacharya, 2006) (Fig. 4a).

156 Deltas also experience channel avulsions at the lobe-level (Slingerland & Smith, 2004). These deltaic
157 avulsions occur within a region of high-water surface slope variability caused by backwater
158 hydrodynamics that are characterized by spatial flow deceleration and deposition during low flows, and
159 flow acceleration and bed scour with high flows (Brooke et al., 2022; Chatanantavet et al., 2012;
160 Chatanantavet & Lamb, 2014). As the backwater zone sets the location for avulsion in deltas
161 (Chatanantavet et al., 2012), they are strongly controlled by hydrodynamics in their receiving basin, like
162 bifurcations. As a result, the delta lobe size is generally consistent and the lobe avulsion node migrates
163 downstream commensurate with shoreline progradation (Ganti et al., 2014), as influenced by flood
164 frequency, sediment supply, or sea-level rise (Brooke et al., 2022). These avulsions episodically rearrange
165 the depocenter at the delta lobe scale, whereas the substantially more frequent bifurcations generate the
166 topology of the delta distributary channel networks (Bentley et al., 2016; Edmonds & Slingerland, 2007).

167 Resultant delta channel networks have a specific angle at which distributary channels bifurcate (Fig.
168 4a) (Coffey & Shaw, 2017), because a channel bifurcation will grow toward an equilibrium angle of 72°
169 to maximize flux at the two channel tips (Coffey & Shaw, 2017; Devauchelle et al., 2012; Ke et al., 2019;
170 Mahon et al., 2024). First described in tributary networks, this theoretical angle arises from diffusive

171 groundwater flow (Devauchelle et al., 2012). Testing of this concept reports bifurcation angles of $70.4^\circ \pm$
 172 2.6° ($n = 9$) in natural deltas (Coffey & Shaw, 2017), and $68.3^\circ \pm 8.7^\circ$ ($n = 21$) (Coffey & Shaw, 2017)
 173 and $74.1^\circ \pm 7.7^\circ$ ($n = 13$) (Federici & Paola, 2003) in experimental deltas.

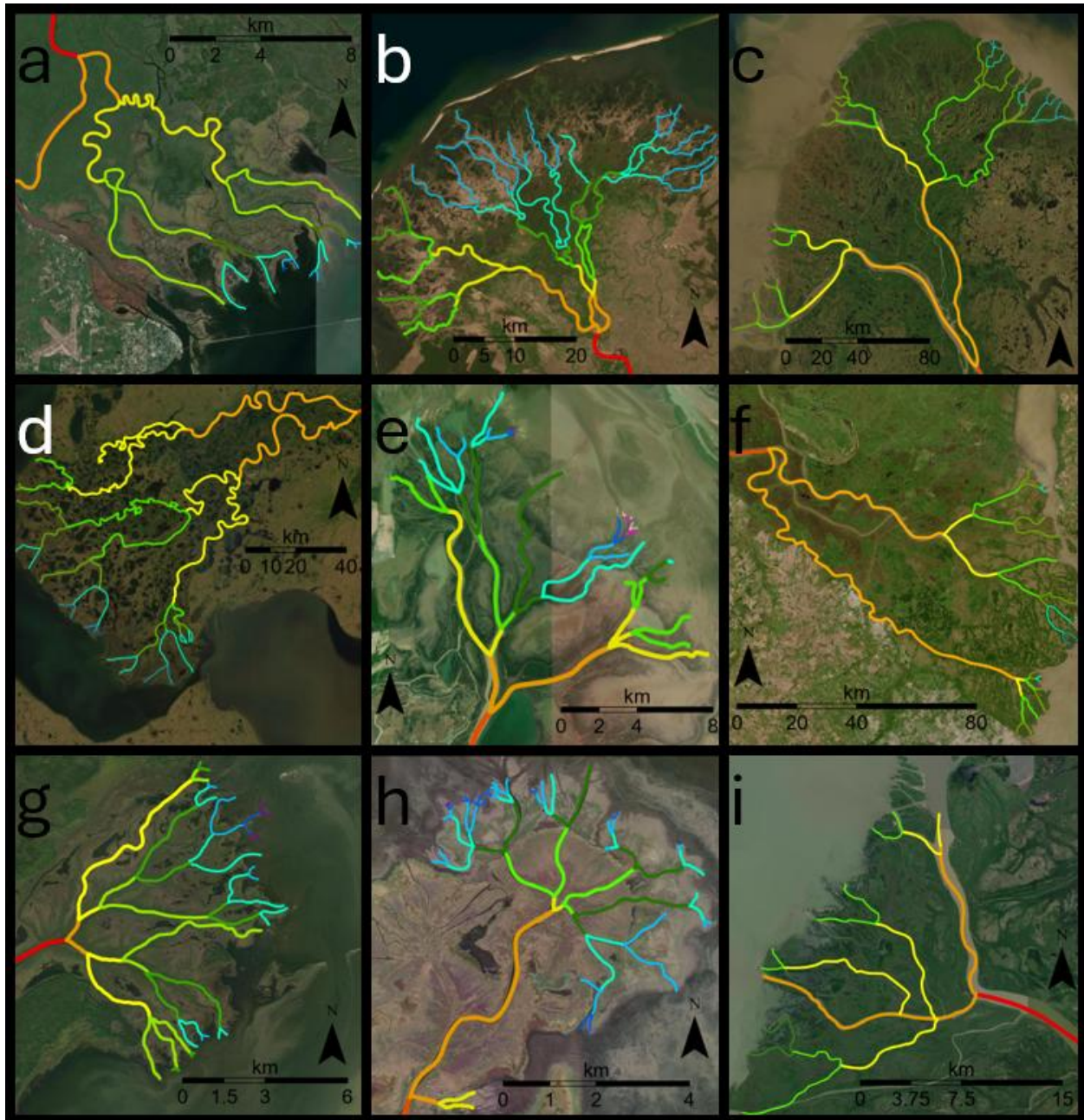


Figure 1: Examples of delta channel networks: (a) Apalachicola, (b) Selenga, (c) Yukon, (d) Kobuk, (e) Poyang Lake, (f) Parana (g) Saskatchewan, (h) Mamawi lake, (i) Slave deltas. The colors indicate channel hierarchy (see Methods). Base imagery from Esri's World Imagery basemap (© Esri, Maxar, Earthstar Geographics, and the GIS User Community).

174 Deltaic channel networks tend to consistently self-organize (Edmonds et al., 2011; Fagherazzi, 2008)
 175 and exhibit a theoretical fractal pattern of decreasing channel widths and lengths associated with
 176 increasing bifurcation order (Edmonds et al., 2011; Edmonds & Slingerland, 2007; Hariharan et al., 2022;

177 Seybold et al., 2017; Wolinsky et al., 2010) (Fig. 4a). Edmonds & Slingerland, (2007) show that channel
178 width trends align with hydraulic geometric scaling: as the discharge of a parent channel divides into the
179 discharge for two resultant daughter channels, the daughter channel dimensions decrease as they scale
180 with bankfull discharge. Channel lengths decrease downstream with each successive bifurcation because
181 the jet momentum flux and consequent average grain transport distance decrease downstream, causing
182 new mouth bar deposition and accompanying bifurcations to occur closer to the previous bifurcation node
183 for a given channel (Edmonds & Slingerland, 2007) (Figs. 4a and 5a).

184 The nature of delta channel networks is further affected by waves and tides (Broaddus et al., 2022;
185 Geleynse et al., 2011; Jerolmack & Swenson, 2007) where the relative strength of river, wave, and tide
186 processes determines whether deltas are river, wave, or tide dominated (Galloway, 1975; Nienhuis et al.,
187 2015, 2018; Paniagua-Arroyave & Nienhuis, 2024; Vulis et al., 2023). Since wave- and tide-*dominated*
188 deltas exhibit distinct morphologies from river-dominated delta and fluvial fan channel networks, they are
189 not considered in this study (See Methods for more information on classification).

190 **2.2 Fluvial Fans**

191 In contrast to deltas where bifurcations and avulsions are strongly controlled by hydrodynamics near
192 a receiving basin of standing water (Brooke et al., 2022; Chatanantavet et al., 2012; Ganti et al., 2014),
193 fluvial fan river avulsions are driven by a topographic slope break (Ganti et al., 2014; Martin & Edmonds,
194 2023). Increased likelihood of avulsions at the fan apex is a consequence of the gradient reduction that
195 triggers in-channel sediment aggradation (Parker et al., 1998). These avulsions result from high channel
196 bed aggradation rates that are considerably higher than on the surrounding floodplains (Pizzuto, 1987).
197 This process causes river channel superelevation which ultimately triggers river avulsions near the fan
198 apex (Bryant et al., 1995; Gearon et al., 2024; Mohrig et al., 2000). Since this slope break controls the
199 location of the fluvial fan's apex, the avulsion node is thus topographically pinned (Ganti et al., 2014) at
200 this abrupt change in gradient, unlike in deltas (Brooke et al., 2022). Partial or full avulsions do occur
201 further downfan, involving local gradient or discharge decreases, or crevassing processes (Assine, 2005;
202 Chakraborty et al., 2010; Donselaar et al., 2013; Gearon et al., 2024) (Fig. 2).

203 Fluvial fan channel networks result through repeated nodal style avulsions that typically shift the
204 primary river to different regions of the fan (Slingerland & Smith, 2004). These avulsions superimpose
205 new channel positions on paleo-channel locations and can split channels by partial avulsions and
206 crevasses. This generates apparent channel "bifurcations" (North & Warwick, 2007) (Fig. 4b). However,
207 as a process, these are not bifurcations related to mouth bar deposition but rather generated by avulsions.
208 Fluvial fan channel networks are predominantly paleo-channel networks rather than active channel

209 networks like in deltas (Chakraborty et al., 2010; North & Warwick, 2007). Multiple channels can
210 actively transmit discharge at partial avulsions, such as during major river floods.

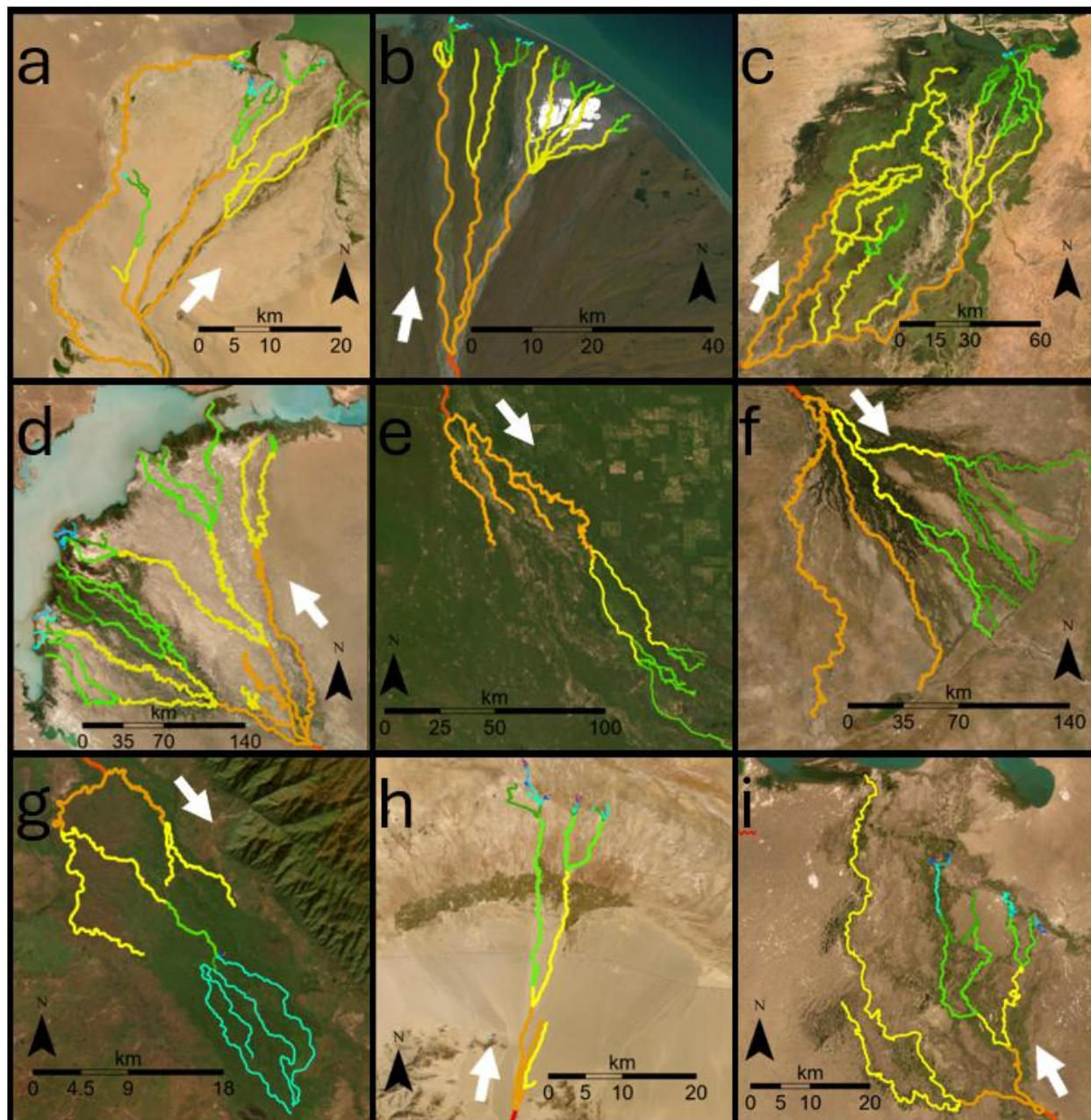


Figure 2: Examples of fluvial fan channel networks: (a) Dzavhan Gol, (b) Kongakut, (c) Niger, (d) Ili, (e) Pilcomayo, (f) Okavango, (g) Shire, (h) Nomon He, and (i) Aksu fans. The colors indicate channel hierarchy (see Methods), and white arrows indicates downfan direction. Base imagery from Esri's World Imagery basemap (© Esri, Maxar, Earthstar Geographics, and the GIS User Community).

211 Downfan decreases in channel width have been well documented in modern and ancient fluvial fans
212 (Davidson et al., 2013; Kelly & Olsen, 1993; Nichols, 1987; Nichols & Fisher, 2007; Owen et al., 2015;
213 Wang & Plink-Björklund, 2019; Weissman et al., 2010), linked to discharge losses to floodplain
214 processes, infiltration into the loose sediments of the fan, and evapotranspiration (Davidson et al., 2013;

215 Hartley et al., 2010; Horton & Decelles, 2001; Weissman et al., 2010). However, some fluvial fan
216 channels have also been shown to widen downstream, possibly due to changes in channel planform or
217 aspect ratio, discharge contribution from groundwater, or discharge capture from adjacent rivers
218 (Chakraborty et al., 2010; Davidson et al., 2013). Fluvial fan channel networks have been studied for
219 qualitative descriptions of channel planform morphology (Davidson et al., 2013; Hartley et al., 2010;
220 Weissman et al., 2010) and scaling relationships (Davidson et al., 2013; Davidson & Hartley, 2014).
221 Modeling establishes a relationship between the fluvial fan shape and avulsion dynamics, like avulsion
222 trigger period and abandoned channel dynamics (Edmonds et al., 2022; Martin & Edmonds, 2023).

223 Fluvial fans are distinct landforms from alluvial fans that feature steep gradients (typically 2–12°),
224 have a relatively small radial distance typically less than 10 kilometers, and lack channel networks (Blair
225 & McPherson, 1994; Moscariello, 2018). Although surface channels may occur on alluvial fans, these are
226 transient features formed by surface erosion, and do not construct alluvial fans, which form by a
227 combination of gravitational and sheet flood processes (Blair & McPherson, 1994; Moscariello, 2018).
228 Thus, alluvial fans are not considered here as they are distinct from fluvial fan channel networks that form
229 by river avulsions.

230 **2.3 Morphometric Criteria for Recognition of Delta and Fluvial Fan Channel Networks**

231 Based on the above differences in delta and fluvial fan morphodynamics, we hypothesize that the
232 morphometric differences in their channel networks can be quantified. Based on prior work, we expect
233 river-dominated delta channel networks to display downstream decreasing channel widths and lengths
234 with increasing bifurcation order (Edmonds & Slingerland, 2007; Seybold et al., 2007; Wolinsky et al.,
235 2010), and have an average channel network angle of approximately 72° (Coffey & Shaw, 2017). These
236 metrics should differ in fluvial fans, because the channel networks are built by avulsions rather than
237 bifurcations. However, delta networks also experience avulsions, and we expect some overlap in the
238 network angles. Below, we test these morphometric criteria on 40 river-dominated delta and 40 fluvial fan
239 channel networks (Fig. 3).

240 **3. Dataset and Methods**

241 Although automated channel mapping tools like ChannelExtractor in TopoToolbox (Schwanghart &
242 Kuhn, 2010) and Rivamap (Isikdogan et al., 2017) exist, these methods rely on either terrain-based flow
243 routing or the detection of active surface water, typically based on spectral characteristics, to delineate
244 river channels. However, fluvial fan channel networks are predominantly composed of paleo-channels
245 that lack both clear topographic expression and surface water signatures. Both delta and fluvial fan
246 channels can also be only a few meters wide, often falling below the spatial resolution of commonly
247 available DEMs and remote sensing imagery. In such settings, the coarse resolution and smoothing of

248 subtle terrain in DEMs, especially in low-relief environments, further limit the effectiveness of automated
249 extraction. As a result, we are constrained to manual digitization, as described below.

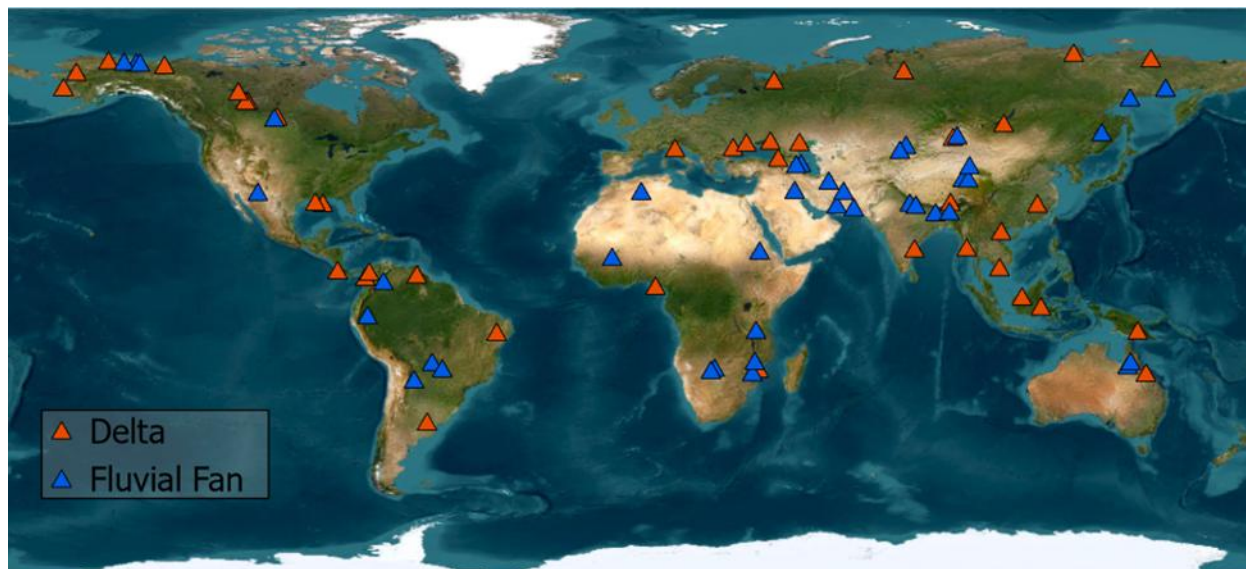


Figure 3: Map of deltas and fluvial fans in this study. Base imagery from Esri’s World Imagery basemap (© Esri, Maxar, Earthstar Geographics, and the GIS User Community).

250 3.1 Channel Order

251 To establish channel order in networks, we follow (Dong et al., 2016). Their method follows a simple
252 rule: bifurcations produce downstream increasing channel order through channels that branch. To be
253 considered a channel of a higher order, the resultant channels must not merge downstream. When a first-
254 order channel bifurcates, two second-order channels develop downstream of this bifurcation. When these
255 two channels subsequently bifurcate, two new pairs of third-order channels form, and so on (Figs. 4a and
256 4b). All channels from the first instance of branching up to and include those that enter a body of water or
257 terminate on land are measured. Identification of bifurcation nodes follows Edmonds et al., (2011), such
258 that the first-order bifurcation for a river channel is the first bifurcation that the channel undergoes (Fig.
259 4a). Although these methods were developed for deltaic channel networks, here we adapt them for fluvial
260 fan networks also (Figs. 4c and 4d). We do not map or measure channels that loop or rejoin downstream,
261 or channels of non-fluvial origin, such as tidal channels or inlets (Smart, 1971; Tejedor et al., 2015) that
262 are not connected to the fluvial distributary channels. We also omit local avulsions on fluvial fans, which
263 generate channels that typically merge downfan (Slingerland & Smith, 2004). Paleo-channels on fluvial
264 fans were recorded where possible. Paleo-channels resembled active channels that exhibit little to no
265 discharge when we mapped the channel networks. We included paleo-channel measurements in fluvial
266 fans because they are ubiquitous in fluvial fans (Hartley et al., 2010), and many of these channels do carry
267 discharge if reactivated during major flood events.

268 3.2 Channel Length and Width Measurements

269 Channel length and width measurements follow Edmonds & Slingerland (2007), where channel
270 length is measured as the distance between two bifurcation nodes in deltas (Fig. 4a). We adopt this
271 methodology also to fluvial fans to measure channel lengths between avulsion nodes (Fig. 4c). The
272 average width of a channel segment is recorded from three separate width measurements: one
273 immediately after a node (w_i), one immediately before the next node (w_f), and one halfway between these
274 two points at the midpoint of the channel segment (w_h) (Figs. 4a and 4c). Channel width measurements
275 were not performed in locations where a channel has locally split into multiple branches that join
276 downstream. In deltas, channel width measurements were recorded based on the width of water present in
277 the channel, as observed in the satellite imagery. For fluvial fans, paleo-channel width measurements
278 were based on the bankfull width, defined by clearly visible channel banks or vegetation boundaries. All
279 channel width measurements were normalized using the initial first-order channel width, following the
280 methodology of Edmonds & Slingerland, (2007). Consequently, the normalized channel width value for
281 first-order channels is always equal to one. First-order channel lengths were measured between the last
282 occurrence of tributary channels and the first channel splitting node and contain no significant value for
283 our study. All channel length measurements (l) were also normalized using the first order channel width
284 measurements according to existing methodologies (Edmonds & Slingerland, 2007; Jerolmack, 2009). As
285 such, the normalized first order channel length values merely reflects our selected methodologies rather
286 than an attributable morphological characteristic.

287 **3.3 Network Angle Measurements**

288 To quantify network angles, we adopt the methodology of Coffey & Shaw, (2017) developed for
289 measuring channel bifurcation angles, which determines the angles of mouth bars formed at the end of an
290 upstream channel. In this methodology, the final channel width directly upstream of a bifurcation (w_f) is
291 set as the length for two limbs of an angle that follows the mouth bar-water contact to measure a
292 bifurcation angle (θ_n) (Coffey & Shaw, 2017) (Fig. 4b). The same methodology is adapted here for fluvial
293 fans (Fig. 4d). In some river deltas, tidal processes cause bifurcation of a channel into three channels
294 instead of two; these are referred to as trifurcations (Leonardi et al., 2013), furcation (Shaw et al., 2018)
295 or polyfurcations (Chamberlain et al., 2018), and a few such measurements are included in the dataset in
296 the very distal portions of deltas where tidal influence is significant. We do not measure angles where
297 channels loop or rejoin downstream of avulsions or bifurcations. In essence, we focus on the morphology
298 of branching channel networks and measure the visible angles between channels or paleo-channels
299 independent of their origin (Fig. 4b and 4d).

300

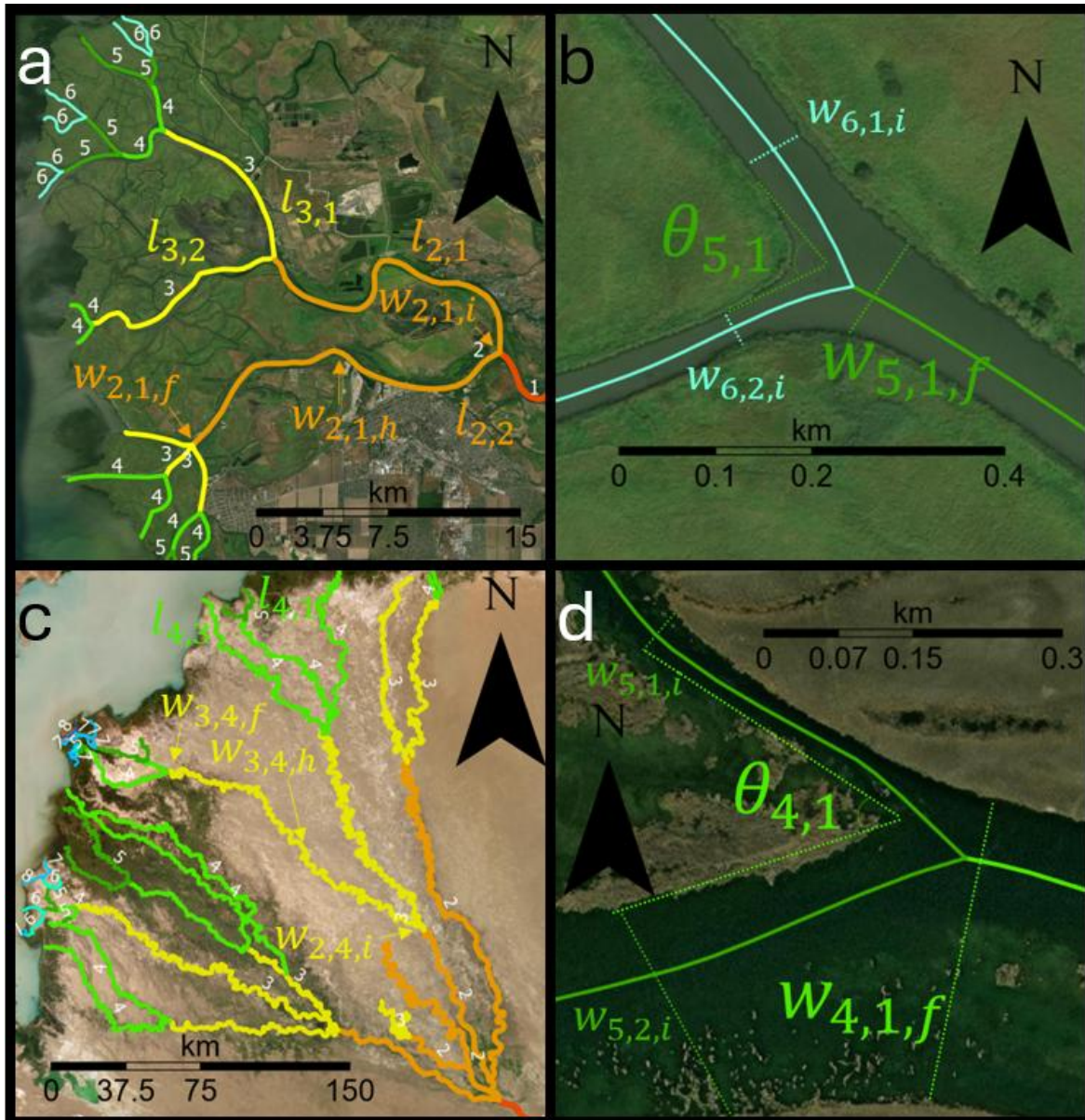


Figure 4: Illustration of (a) channel order, length, and width and (b) bifurcation angle measurements in deltas (Don delta). Illustration of (c) channel order, length, and width and (d) divergence/crossover angle measurement (Ili fan). Arrows point to locations of w_i = initial channel width, w_h = midpoint channel width, w_f = final width measurements. The w_f is set as the length of two limbs that track along the edges of the mouth bar. θ_n corresponds to the bifurcation or divergence/crossover order. Base imagery from Esri's World Imagery basemap (© Esri, Maxar, Earthstar Geographics, and the GIS User Community).

301 3.4 Global Delta and Fluvial Fan Channel Network Database

302 To test the applicability of the proposed criteria, we selected 40 river-dominated deltas and 40
 303 fluvial fans (Fig. 3 and Supplementary Data) to be mapped using composite satellite data (ESRI, 2025).
 304 These landforms were selected from a diverse range of hydroclimatic, topographic, and basal conditions
 305 from across the world (Fig. 3). Only river-dominated deltas are included in the dataset, because wave-and

306 tide-dominated delta morphology is distinct from that of fluvial fans. All deltas have been identified as
307 such by prior work (Broaddus et al., 2022; Galloway, 1975; Hartley et al., 2010; Leier et al., 2005;
308 Nienhuis et al., 2015, 2018; Vulis et al., 2023), and display active discharge based on satellite imagery.
309 The river dominance of deltas and the presence of tide- or wave-influence was determined using the
310 established principles of process-based delta classification (Broaddus et al., 2022; Galloway, 1975;
311 Nienhuis et al., 2015, 2018; Paniagua-Arroyave and Nienhuis 2024; Vulis et al., 2023). However,
312 categorical discrepancies exist between these different classification approaches. To clarify our
313 terminology, we define “dominated” versus “influenced” deltas as follows. Wave-dominated deltas (e.g.
314 São Francisco, Eel) are characterized by strandplanes and a complete absence of bifurcations; these deltas
315 are excluded from our study. Wave-influenced deltas still possess morphological features such as
316 strandplains, but exhibit clear, measurable channel bifurcations and are included in our study. Similarly,
317 tide-dominated deltas (e.g. Fly, Yangtze) have a limited number of channels that widen substantially
318 seaward, whereas tide-influenced deltas such as the Yukon (Fig. 1c) exhibit channel widening only in the
319 most distal channels (Xu & Plink-Björklund, 2023). In practice, we combine these parameters with
320 established classifications (Broaddus et al., 2022; Galloway, 1975; Nienhuis et al., 2015, 2018; Paniagua-
321 Arroyave & Nienhuis, 2024; Vulis et al., 2023) to categorize the deltas in our study. Please refer to the
322 Supplementary Data for information regarding our classification of each delta. We test the effects of tide-
323 and wave-influence on the morphometric criteria by comparative analyses.

324 Fluvial fans were located using their apex coordinates from the global fluvial fan database of
325 Hartley et al., (2010). This database also includes data on fluvial fan length, gradient, termination style
326 (e.g. axial, contributory, lacustrine, marine, playa, desert/dune, and wetland). Termination styles refer to
327 the environment where the fluvial fan terminates: for instance, a contributory-termination style denotes
328 that the landform channels switch from distributary to contributory at the toe of the fan, while axial fans
329 are classified when the main channel forms a confluence with an axial fluvial system (Hartley et al.,
330 2010). We also subdivided delta termination styles in lakes and oceans. To test the robustness of our
331 methodology, we analyze whether the landform size, gradient, termination style, or wave- and tide-
332 influence in deltas affect the results.

333 **3.5 Mapping with ArcGIS Pro**

334 Delta and fluvial fan channel networks were mapped using ArcGIS Pro software (Version 3.2.1)
335 (Fig. 1, 2, and 4). Two feature classes were created: one for deltas and one for fluvial fans. Each delta or
336 fluvial fan landform was then individually mapped as a shapefile layer under the corresponding feature
337 class. The shapefiles for channel networks were created as polyline features, which allow users to
338 manually trace individual river channel segments while automatically recording line lengths. Channel
339 widths and angles were measured using the line and angle measurement tools in ArcGIS Pro. All data was

340 recorded in the attribute table for each landform. This data was organized into Excel documents and
341 subsequently converted to Python- and Pandas- readable CSV files (Supplementary Data).

342 One limitation of our methodology is uncertainty regarding the timing of satellite image
343 acquisition relative to precipitation events. Precipitation increases channel discharge, thereby increasing
344 measured channel widths, particularly for fluvial fans in arid environments. Such events can also
345 reactivate partial avulsions and crevasses, which can potentially increase the apparent number of
346 channels. However, none of the selected systems exhibited observable seasonal or large-scale discharge
347 changes across their channel networks attributable to different timings in data collection. Additionally,
348 because this study relies on values normalized to the initial channel width, the effects of seasonal
349 variability on channel width measurements are minimized.

350 **3.6 Code and Statistics**

351 Kolmogorov-Smirnov and Shapiro-Wilk tests were first applied to determine whether the data are
352 normally distributed. Levene's test was used to test differences in variances of populations that do not
353 exhibit a normal distribution (Trauth, 2006). Independent samples or Welch's t-test were then applied to
354 test for a difference in means for populations with similar and dissimilar variances, respectively, while
355 one-sample t-tests were used to test comparisons of a subgroup against the overall population mean
356 (Trauth, 2006). For this study, a p-value less than 0.05 (5% significance level) suggests that the two
357 population distributions, variances, or means are not similar. Data confidence intervals were calculated
358 according to Mendenhall et al., (2012). Data analysis and visualization were performed using Python.
359 Open-source data visualization libraries Matplotlib (Hunter, 2007), NumPy (Harris et al., 2020), SciPy
360 (Virtanen et al., 2020), and Seaborn (Waskom, 2021) were utilized.

361 **4. Results**

362 **4.1 Delta and Fluvial Fan Channel Network Angles**

363 The mean channel network angle (θ_d) in deltas is 73.8° with a 95th percentile confidence interval of \pm
364 1.9° ($n = 528$) (Fig. 5a). The mean channel network angle (θ_f) in fluvial fans is $55.0^\circ \pm 2.0^\circ$ ($n = 520$)
365 (Fig. 5b). The delta and fluvial fan network angle populations are not normally distributed according to
366 both Kolmogorov-Smirnov (KS) and Shapiro-Wilk (SW) tests, with p-values less than 0.05. Levene's test
367 for statistical difference in variances also results in a p-value less than 0.05, suggesting population
368 variances are statistically different. A subsequent independent sample t-test suggests the means of delta

369 and fluvial fan angle populations are statistically different, with a p-value less than 0.05. All statistical
 370 results are recorded in Supplementary Table 1 in the Supplementary Information.
 371

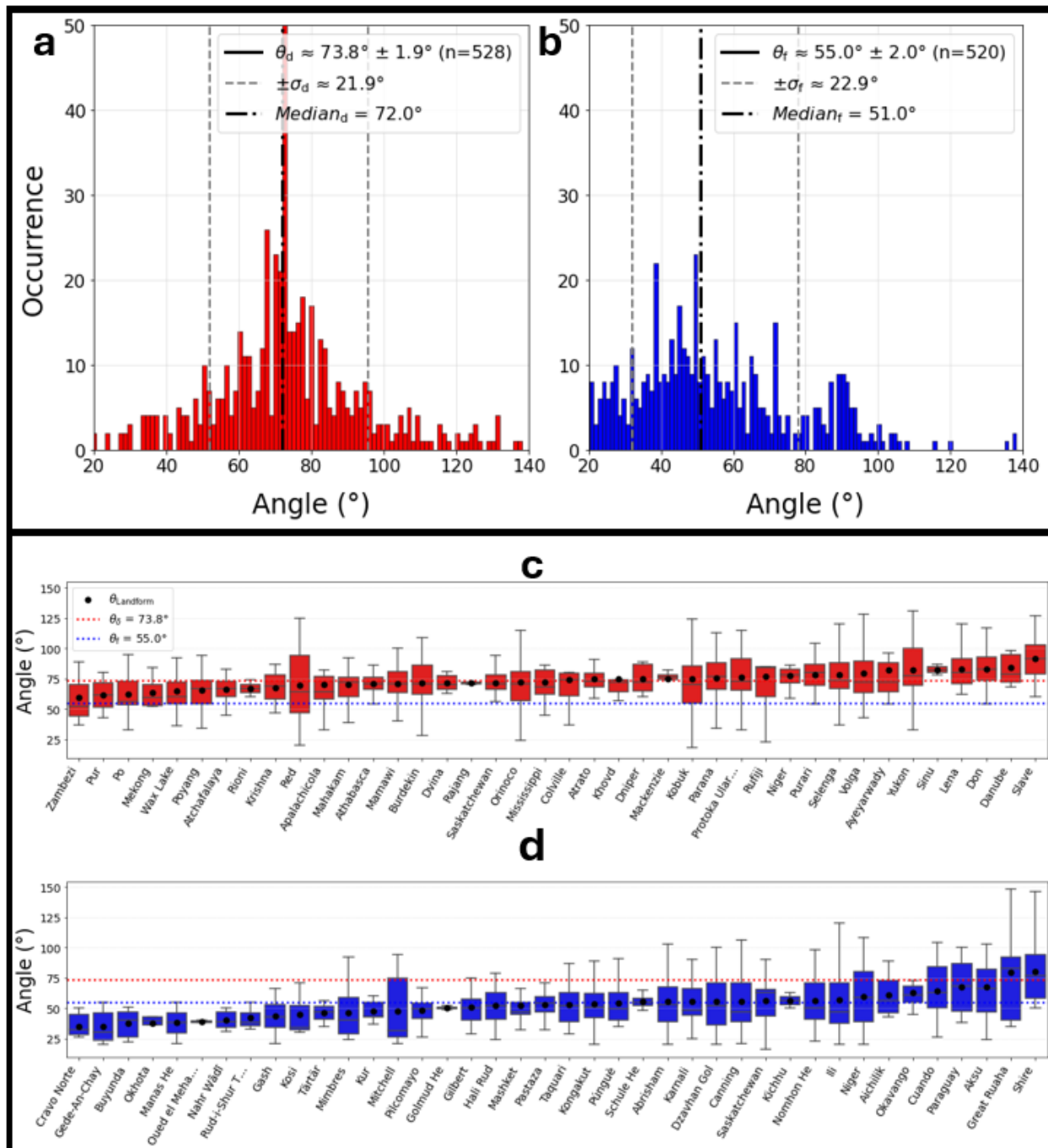


Figure 5: Histograms depicting distributions of (a) delta angles with mean delta angle (θ_d), its standard deviation (σ_d) and median and (b) fluvial fan angles with mean fan angle (θ_f), its standard deviation (σ_f), and median displayed. Box-and-whisker plot displaying the mean angle for each delta (c) and fluvial fan (d) landform ($\theta_{Landform}$).

372 We also reviewed the mean network angle of each individual delta and fluvial fan (θ_{Landform}) (Figs. 5c
 373 and 5d), and these analyses reveal some overlap. All fluvial fans have mean angle values less than 60° ,
 374 except for six landforms, or 15% of fluvial fans in this study. Four of these landforms have mean angles
 375 larger than 60° (60.8° , 63.2° , 67.7° , 67.9°), and two larger than the delta mean of 73.7° (79.6° , 80.1°). All
 376 individual deltas have mean network angles larger than 60° , except for one delta (59.3°). There are also
 377 three deltas with mean angles around 60° (61.5° , 62.4° , 63.3°).

378 The distribution of delta angles grouped by order (Fig. 6a) yields no strong trends for mean angle in
 379 deltas. Seventh and tenth order channels have slightly lower mean angle values at 65° and 67° , but these
 380 higher-order groups have low sample sizes ($n = 3$; $n = 8$) (Fig. 6a). The distribution of fluvial fan angles
 381 grouped by order does yield a trend: the mean angle for first- through third-order channels (θ_1 , θ_2 , and θ_3
 382 in Fig. 6b) is between $47 - 50^\circ$ and increases to $61 - 63^\circ$ for fourth- through eighth-order channels, and to
 383 66° for ninth-order angles ($n = 6$) ($\theta_4 - \theta_9$ in Fig. 6b). In contrast to the unimodal distribution of delta
 384 angles, the distribution of higher-order fluvial fan angles is bimodal, with a dominant peak near 50° and a
 385 secondary peak around $80 - 100^\circ$ (Fig. 6b).

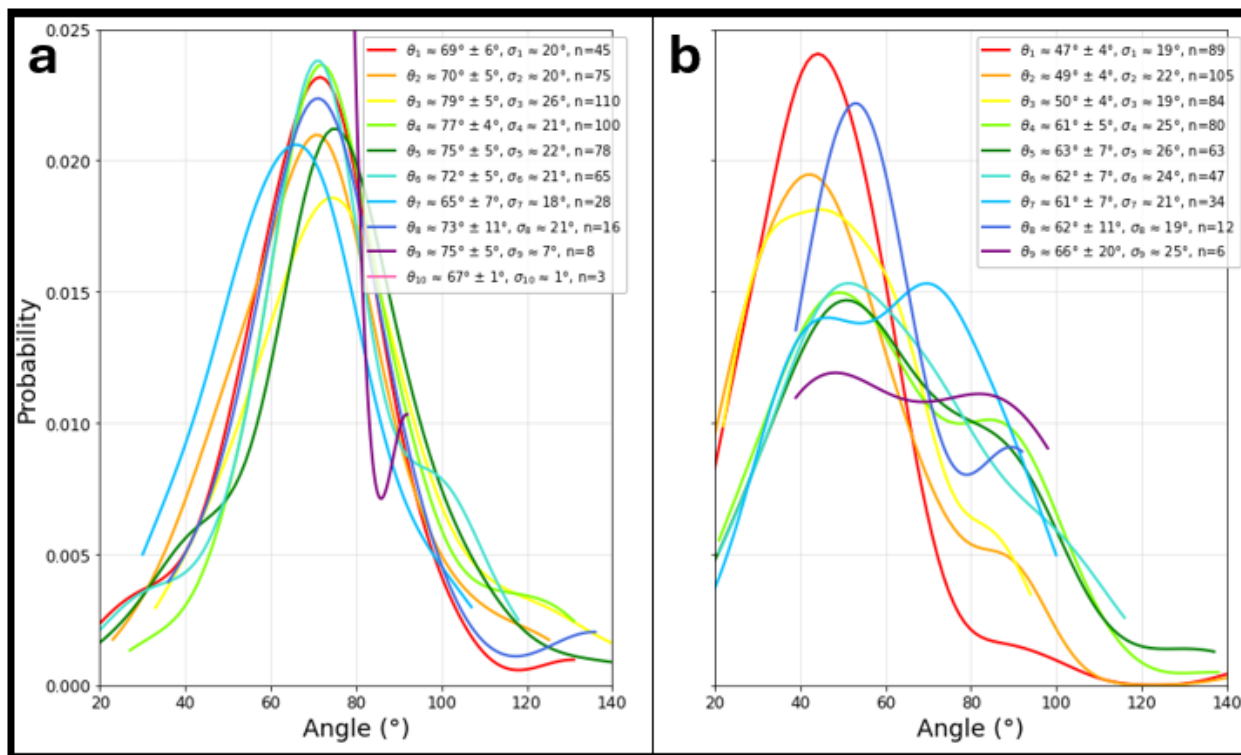


Figure 6: Distribution of (a) delta bifurcation angles, and (b) fluvial fan divergence/crossover angles grouped by order (θ_n) with the 95th percent confidence interval. (σ_n) = denotes standard deviation. n denotes sample size.

386 All deltas in this analysis are river-dominated deltas, however some are tide- or wave-influenced (See
 387 Section 3.4 and Supplementary Data). Grouping deltas by process regime shows that the mean bifurcation

388 angle for the 19 river-dominated deltas ($\theta_R = 73.4^\circ \pm 2.2^\circ$, $n = 375$), for the 16 tide-influenced deltas ($\theta_t =$
 389 $75.6^\circ \pm 3.9^\circ$, $n = 139$), and for the 5 wave-influenced deltas ($\theta_w = 67.1^\circ \pm 10.1^\circ$, $n = 14$) (Fig. 7a). The
 390 river-dominated and tide-influenced delta angle means are not statistically different from the mean angle
 391 for the whole delta population (Supplementary Table 1). The wave-influenced delta angles were omitted
 392 from this statistical analysis due to a small sample size ($n = 14 < 30$).

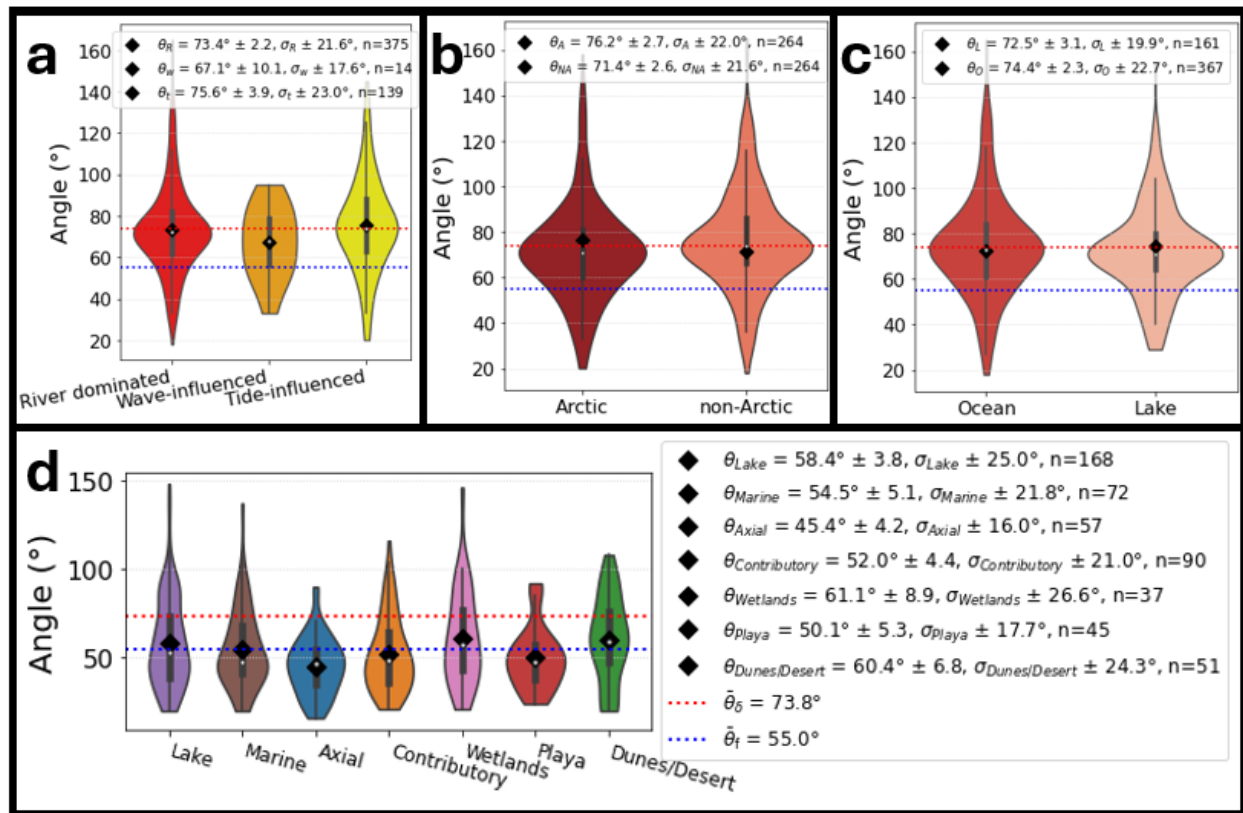


Figure 7: Violin plots depicting angle distributions for (a) delta process regime: river dominated (θ_R), wave-influenced (θ_w), and tide-influenced (θ_t), (b) deltas in non-Arctic (θ_{NA}) and Arctic (θ_A) climates, (c) ocean terminated deltas (θ_O) and lake terminating deltas (θ_L), and (d) fluvial fan termination styles. All mean angle values have a corresponding 95th percent confidence intervals, standard deviation (σ), and sample count (n).

393 Many delta angle measurements in this dataset come from Arctic deltas. The comparison between
 394 Arctic and non-Arctic deltas shows that Arctic deltas have a larger mean angle ($\theta_A = 76.2^\circ \pm 2.7^\circ$, $n =$
 395 264) than non-Arctic deltas ($\theta_{NA} = 71.4^\circ \pm 2.6^\circ$, $n = 264$) (Fig. 7b). There is a statistically significant
 396 difference in means between Arctic and non-Arctic deltas (Supplementary Table 1). Grouping deltas by
 397 termination style (Fig. 7c) shows that lake-terminating deltas have slightly smaller mean angles than those
 398 that terminate in oceans ($\theta_L = 72.5^\circ \pm 3.1^\circ$, $n = 161$ versus $\theta_O = 74.4^\circ \pm 2.3^\circ$, $n = 367$), but these
 399 differences are not statistically significant compared to the whole delta population (Supplementary Table
 400 1).

401 Grouping fluvial fans by their termination style shows some differences (Fig. 7d), where the mean

402 angles vary from a low of $\theta_{\text{Axial}} = 45.4^\circ \pm 4.2^\circ$ ($n = 57$) for axial-terminating fluvial fans to $\theta_{\text{wetlands}} = 61.1^\circ$
403 $\pm 8.9^\circ$ ($n = 37$) for wetland-terminating fans (Fig. 7d). All fluvial fan termination types, except for axial-
404 terminating fans, exhibit population means that are statistically similar to the overall fluvial fan
405 population (Supplementary Table 1). However, each termination style is represented by only 4 to 6
406 landforms, limiting the statistical power of comparisons and generalizations, despite the relatively robust
407 measurement numbers in wetland ($n = 37$), playa ($n = 45$), dunes/desert ($n = 51$), and axial-terminating
408 fans ($n = 57$). There also appears to be some discrepancies in Hartley et al., (2010)'s assignment of
409 termination types, such as referring to playa fans as lacustrine or ocean fans as contributory. We also
410 tested whether landform size (Supplementary Fig. 1) and gradient (Supplementary Fig. 2) affect the
411 channel network angles, and these analyses yield no trends, supporting the robustness of our
412 methodology.

413 **4.2 Channel Lengths and Widths**

414 Normalized channel length and width measurements reveal morphological differences between
415 fluvial fan and delta channels. Both landform types show non-linear decreases in these values with
416 increasing channel order (Fig. 8). Statistical analyses confirm that the overall means for normalized
417 channel length and width differ significantly between fluvial fans and deltas (Supplementary Table 1).
418 Fluvial fan channels are generally an order of magnitude longer than delta channels, with a mean
419 normalized length of 147.09 compared to 17.18 for deltas (Figs. 8a and 8c). In contrast, delta channels
420 tend to be slightly wider, with a mean normalized width of 0.40 compared to 0.26 for fluvial fans (Figs.
421 8b and 8d).

422 Comparing the normalized dimensions by channel order (Fig. 9) reveals additional trends. The
423 normalized channel widths of lower-order fluvial fan channels (orders 1–5) are significantly longer, and
424 the channel shortening rate is higher compared to deltas (Fig. 9a). The normalized lengths become very
425 similar in orders 7–8, then diverge again for the higher orders where the fluvial fan channel lengths are
426 somewhat longer, but the channel shortening rates are higher in deltas. Normalized channel widths show
427 significant differences for orders 2–8, but not for 9–11. Only a few landforms have channels with orders
428 exceeding 9. Fluvial fan narrowing rates are very high from order 1 and 2, and very low in orders 7–10
429 (Fig. 9b). The narrowing rates are more uniform in deltas.

430 When comparing individual deltas by process regime, both tide- and wave-influenced deltas have
431 significantly higher mean normalized channel widths relative to the overall delta population
432 (Supplementary Fig. 3 and Supplementary Table 1).

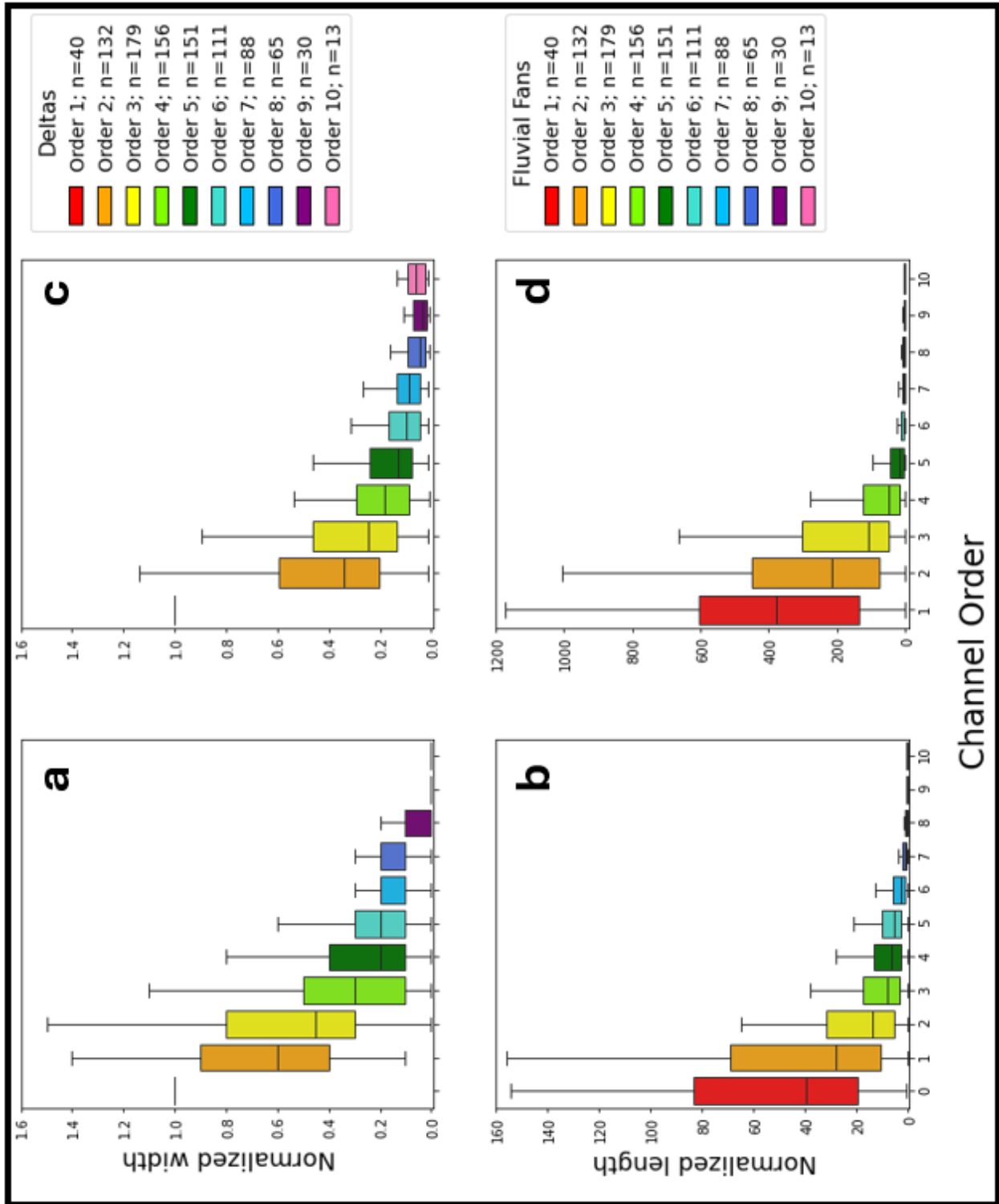


Figure 8: Box and whisker plots illustrating normalized delta channel widths (a) and lengths (b) and normalized fluvial fan channel widths (c) and length (d), plotted by channel order. Note the significant difference in normalized channel length scales for subplots b and d.

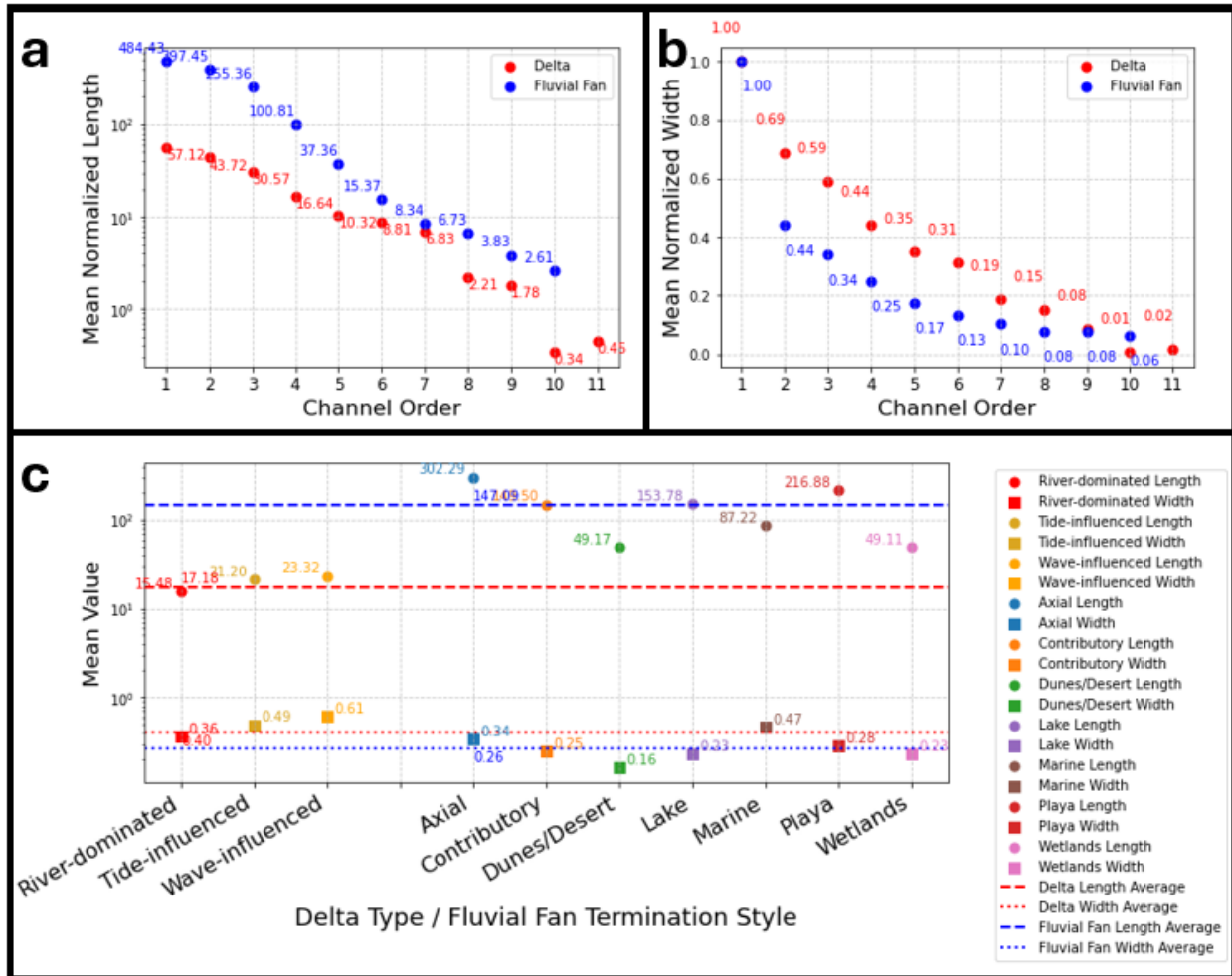


Figure 9: Mean normalized delta and fluvial fan channel (a) lengths by order and (b) width values by order. (c) Mean channel length and width values for different types of deltas and fluvial fan termination styles.

434 Comparison by fluvial fan termination styles shows that axial- and playa-terminating fans exhibit
 435 longer mean normalized channel lengths compared to the whole fluvial fan population, whereas
 436 dunes/desert-, marine-, and wetland-terminating fans have shorter mean lengths (Supplementary Fig. 3
 437 and Supplementary Table 1). Contributory- and lake-terminating fans do not differ significantly from the
 438 overall mean. Regarding normalized channel widths, axial- and marine-terminating fans have wider
 439 channels, while dunes/desert-terminating fans are narrower. Normalized width values for contributory-,
 440 lake-, playa-, and wetland-terminating fan channels show no difference from the overall population mean
 441 (Supplementary Fig. 3 and Supplementary Table 1). Statistical analyses of channel length and width were
 442 not conducted for different fluvial fan termination styles due to insufficient sample sizes ($n < 30$) in most
 443 categories.

444

445 **5. Discussion**

446 **5.1 Effectiveness of Morphometric Criteria in Distinguishing Deltas and Fluvial Fans**

447 The mean channel network angles are distinctly different in deltas and fluvial fans by 20°, and this
448 statistically significant difference is a useful criterion in distinguishing these two landform types. While
449 some overlaps exist at the landform level, these cases are relatively limited, where 15% of fluvial fans in
450 this dataset have a mean angle larger than 60° (Fig. 5d) and 10% of deltas have a mean angle less than
451 64° (Fig. 5c). These findings support the utility of mean branching angles as a distinguishing metric
452 between deltas and fluvial fans. However, some degree of uncertainty remains, and additional criteria are
453 necessary for more robust distinction.

454 An additional criterion is the distribution of mean angles by channel order, where fluvial fans have
455 increased mean angles and a bimodal distribution in orders 4–8 (Fig. 6). Other supportive criteria may be
456 the differences in values and distributions of the normalized channel lengths and widths (Figs. 8 and 9),
457 but the low sample numbers do not allow us to test these criteria by individual landforms. A useful
458 criterion would be to link channel narrowing with the bifurcation and avulsion nodes. In deltas, the
459 downstream channel narrowing occurs in a stepwise manner at the bifurcation nodes, whereas in fluvial
460 fans this decrease should be gradual and not linked to the node positions where full avulsions occur. Our
461 data was collected in a manner that does not permit these analyses.

462 A potential source of overlap in the delta and fluvial fan channel network mean angles is that not all
463 measured angles in deltas are bifurcation angles, as deltas also experience avulsions (e.g., Fig. 1e). A
464 closer inspection of the four deltas with low mean network angles reveals that each contains very few
465 measurements ($n = 3$, $n = 4$, $n = 6$, $n = 7$). In these cases, the limited sample size allows the rarer avulsion
466 angles to affect the mean values more strongly. Also, fluvial fans that terminate in a lake or ocean may
467 have terminal channels that form due to mouth bar deposition and channel bifurcation. However, we do
468 not believe these instances affect our results since we do not see that lake- or marine-terminating fans
469 exhibit higher mean angles (Fig. 7d).

470 Examining fluvial fans with high mean angles shows that these are low-gradient wetland fans, where
471 the avulsion angles tend to be wider as a function of avulsion mechanisms (see Discussion below).
472 However, they may also suggest methodological limitations. While the local avulsion angles in low-
473 gradient wetland fans are wide (measured the final channel width directly upstream of a bifurcation (w_f)
474 as the length for two limbs of an angle), angles between the longer channel reaches are considerably
475 narrower (Supplementary Fig. 4). This channel reach angle discrepancy is consistent with similar channel
476 reach angle measurements from (Coffey & Shaw, 2017). We plan to further develop angle measurement
477 methods to capture both the local and the reach-scale angles in future work. It is also important to discuss
478 the limitations of the applied methodologies in the context of the results. Our channel network
479 methodologies are designed for delta channel networks, and exclude channels that merge downstream,

480 which can exclude many potential measurements from fluvial fans in situations where their channels
481 merge downfan.

482 In summary, this initial attempt to distinguish deltas and fluvial fans demonstrates that quantifying
483 channel network angles, and trends in normalized channel widths and lengths provide efficient criteria.
484 However, we also show that sample sizes are important for accurate recognition of landforms, and
485 collecting a sufficient number of angle measurements ($n \gtrsim 10$) can help account for the infrequent
486 avulsion in deltas or bifurcation in fluvial fans. While each metric is informative on its own, the
487 combination of branching angles, branching angle trends, and normalized channel lengths provides the
488 clearest distinction between deltas and fluvial fans.

489 **5.2 Processes that determine delta and fluvial fan channel network angles**

490 While the 72° mean bifurcation angle can be explained by flow patterns at channel tips well-
491 explained by diffusive processes (Coffey & Shaw, 2017), there is currently no established explanation for
492 the approximately 55° mean network angle in fluvial fans. In deltas, bifurcation as a process is the
493 product of sedimentation from turbulent jets that form at the mouths of rivers entering basins (Bates,
494 1953; Coffey & Shaw, 2017; Edmonds & Slingerland, 2007; Fagherazzi et al., 2015; Jerolmack &
495 Swenson, 2007; Wright, 1977). Once a mouth bar is formed, the flow through the distributary channel
496 bifurcations can be modeled as diffusive flow (Coffey & Shaw, 2017), and the resulting critical angle of
497 72° represents a stable morphology for the bifurcation as it grows in a diffusive groundwater field
498 (Devauchelle et al., 2012; Ke et al., 2019). The slightly larger network angles in Arctic deltas may reflect
499 environmental influences such as ice cover, permafrost, or limitations on overbank flow (Lauzon et al.,
500 2019; Piliouras et al., 2021; Walker, 1998).

501 River avulsions are set up by channel superelevation (Mohrig et al., 2000), or when the slope down
502 the flanks of the channel provides a steeper descent than the existing river channel (Slingerland & Smith,
503 1998; Törnqvist & Bridge, 2002). Avulsions result from channel bed aggradation that reduces the channel
504 capacity (Bryant et al., 1995). Once an avulsion is triggered and full or partial river flow exits the channel,
505 a new channel is generated by surface runoff erosion. Thus, the prevailing topographic gradient would
506 tend to keep the nearby flows more focused in a slope-parallel direction, resulting in narrower network
507 angles compared to bifurcations (Fig. 5b).

508 The contrast between diffusion-dominated and surface runoff erosion-dominated processes in shaping
509 delta versus fluvial fan channel network topology is further supported by tributary channel network
510 analyses that originally defined the critical angle of 72° (Devauchelle et al., 2012). Tributary channel
511 network analyses show that the mean tributary angle of 72° only occurs in humid catchments with high
512 groundwater recharge, where tributary networks are shaped by groundwater diffusion (Seybold et al.,

513 2017). In contrast, the mean tributary network angle is 45° in arid landscapes where surface runoff
514 dominates (Seybold et al., 2017), or is even lower in the driest catchments (Seybold et al., 2018).

515 Fluvial fan gradient decreases progressively downstream (e.g. Chakraborty et al., 2010), such that
516 higher gradients near the fan apex likely generate more acute angles, whereas the very low gradients near
517 the toe of the fan would allow for wider angles. This trend likely explains the downstream increase in
518 fluvial fan network angles and the emergence of the second, wider peak in higher order channels (Fig.
519 6b). Furthermore, avulsion mechanisms have been shown to change from channel superlevation in
520 upstream river reaches, where river gradients are steeper, to gradient advantage in downstream low-
521 gradient reaches (Gearon et al., 2024). In these low-gradient zones, crevassing processes can produce
522 high-angle deviations with the angle values around 90° (Rahman et al., 2022). Avulsion angles above
523 100° have been measured in meandering rivers on low-gradient floodplains with vegetation (see Rahman
524 et al., 2022). These effects may be important controls in the fluvial fan channel networks in low-gradient
525 vegetated wetlands. Reitz & Jerolmack, (2012) show that abandoned paleo-channel reoccupation may
526 control new avulsion positions, and paleo-channel density is highest in the narrower fan apex. Avulsion
527 angles may also change over time due to evolving channel width ratios (Morais & Montanher, 2022), or
528 may be affected by a critical angle or bend curvature (Yang, 2020). Future work targeting how avulsion
529 morphology evolves downfan would provide important insight into the mechanisms driving the observed
530 increase in angles downstream.

531 We thus conclude that the distinction between deltaic and fluvial fan channel network angles arises
532 from the dominant formative processes: diffusive flow in deltas versus surface runoff erosion in fluvial
533 fans. Furthermore, in fluvial fans, network angles appear to be negatively correlated with surface
534 gradients, with lower gradients allowing for wider avulsion angles.

535 **5.3 Ancient deltas and fluvial fans**

536 Our proposed methodology could also be used to distinguish ancient fluvial fans and deltas, for
537 instance in seismic datasets, where only delta channel network angles have been quantified before
538 (Mahon et al., 2024). Our results confirm the prior modern data (Chakraborty et al., 2010) and recent
539 modeling outcomes (Martin & Edmonds, 2023), and help to eliminate a discrepancy in plan-view versus
540 cross-sectional fluvial fan facies models (Plink-Björklund, 2021). Namely, earlier work suggested
541 bifurcations as a key mechanism driving fluvial fan formation (Friend, 1978; Kelly & Olsen, 1993;
542 Weissman et al., 2010), probably due to downstream channel narrowing. However, this hypothesis
543 contradicts the stratigraphic data that indicate that proximal fans consist of amalgamated channel deposits
544 (Chakraborty et al., 2010; Kelly & Olsen, 1993; Nichols & Fisher, 2007; Singh et al., 1993; Weissman et
545 al., 2013) – a pattern consistent with frequent avulsions (Chakraborty et al., 2010; Singh et al., 1993).

546 **5.4 Sensitivity of Deltas and Fluvial Fans to Global Change**

547 Deltas and fluvial fans differ significantly in their vulnerability to natural hazards and in their
548 responses to global change. Deltas are highly vulnerable to coastal hazards and sea level rise (Giosan et
549 al., 2014; Syvitski et al., 2009). Rising sea-levels will not only inundate deltaic distributary networks, but
550 also cause a landward migration of the avulsion node corresponding with the landward shift of the
551 backwater zone (Brooke et al., 2022; Chatanantavet et al., 2012; Ganti et al., 2014). This process reduces
552 sediment delivery to shorelines, accelerating the effects of sea-level rise. However, changes in land use
553 and changing precipitation patterns which increase sediment supply could complicate the picture by
554 shifting delta avulsion sites seaward (Brooke et al., 2022). In contrast, fluvial fans are controlled by
555 upstream morphodynamics, where the fan location (apex) is pinned by a steep topographic break (Brooke
556 et al., 2022; Ganti et al., 2014; Martin & Edmonds, 2023). For coastal fans, sea-level rise and coastal
557 erosion would affect the fan toes, however the avulsion node at the fan apex and sediment deposition
558 across most of the fan surface would not be affected, making fluvial fans significantly less vulnerable to
559 drowning.

560 Both deltas and fluvial fans are affected by reduced sediment supply due to river damming and
561 artificial levees (Blum & Roberts, 2009; Giosan et al., 2014; Nienhuis et al., 2020; Paola et al., 2011;
562 Syvitski et al., 2009). However, fluvial fans are highly sensitive to the water and sediment supply
563 changes, such as changes in precipitation patterns (Assine et al., 2014; Hansford & Plink-Björklund,
564 2020; Leier et al., 2005). Increases in extreme precipitation cause a significant increase in avulsion
565 frequency and crevassing splay formation (Morón et al., 2017), because large fluctuations in river
566 discharge, such as during extreme precipitation events, are avulsion-triggering events (Jones & Schumm,
567 1999). Indeed, fluvial fans have been shown to be highly sensitive to such changes, where fluvial fan
568 activation and deactivation cycles have been linked to millennial-scale changes in monsoon intensity or
569 precipitation patterns (Assine et al., 2014; Fontana et al., 2014, Latrubesse et al., 2012).

570 **6. Conclusions**

571 This study demonstrates that river-dominated delta and fluvial fan channel networks can be
572 distinguished using quantitative morphometric criteria derived from their channel network topology.
573 Deltaic networks are primarily shaped by bifurcation processes, resulting in mean bifurcation angles of
574 approximately 74° , consistent with diffusion-dominated growth. In contrast, fluvial fan topology is
575 shaped by channel avulsions, producing narrower mean network angles near 55° , indicative of surface
576 runoff processes. Fluvial fan network angles tend to widen downstream, likely due to decreasing gradients
577 and avulsion style shifts, while delta angles remain relatively consistent, reflecting persistent bifurcation
578 processes. Both channel networks display downstream reductions in channel length and width with
579 increasing channel order, but the fluvial fan networks are characterized by significantly longer and
580 somewhat narrower channels when normalized.

581 These differences not only support the use of network morphology as a diagnostic tool for
582 identifying ancient fluvial fans and deltas in the stratigraphic record or other planetary bodies but also
583 provide insights into their differing sensitivities to environmental change.

584

585 **Code Availability**

586 The Python code used for data analysis and figure generation was created and run in Jupyter
587 Notebook version 6.4.8 (Anaconda distribution).

588

589 **Data Availability**

590 Morphological data collected in this study are available at <https://github.com/lukegezovich/Delta-and-Fluvial-Fan-Networks>.

592

593 **Competing Interests**

594 The authors declare that they have no conflict of interest.

595

596 **Acknowledgments**

597 We thank Kamini Singha, Lesli Wood, and Wendy Zhou for their constructive feedback that helped
598 improve earlier versions of this manuscript. We also thank John Shaw, Ellen Chamberlin and an
599 anonymous reviewer for their helpful comments on the present versions of the manuscript.

600

601 **Financial Support**

602 Luke Gezovich thanks the American Association of Petroleum Geologists (AAPG) Foundation John &
603 Erika Lockridge Grant, the American Institute of Professional Geologists (AIPG) William J. Siok Graduate
604 Scholarship, the Colorado Scientific Society (CSS), the Rocky Mountain Association of Geologists
605 (RMAG), and the Society for Sediment Geology (SEPM) for providing funding to support this research.

606

607

608

609

610

611

612

613

614 **References**

- 615 Allen, P. A. (2008). Time scales of tectonic landscapes and their sediment routing systems. *Geological*
616 *Society, London, Special Publications*, 296(1), 7–28. <https://doi.org/10.1144/SP296.2>
- 617 Assine, M. L. (2005). River avulsions on the Taquari megafan, Pantanal wetland, Brazil. *Geomorphology*,
618 70(3–4), 357–371. <https://doi.org/10.1016/j.geomorph.2005.02.013>
- 619 Assine, M. L., Corradini, F. A., Pupim, F. D. N., & McGlue, M. M. (2014). Channel arrangements and
620 depositional styles in the São Lourenço fluvial megafan, Brazilian Pantanal wetland. *Sedimentary*
621 *Geology*, 301, 172–184. <https://doi.org/10.1016/j.sedgeo.2013.11.007>
- 622 Axelsson, V. (1967). The Laitaure Delta: A Study of Deltaic Morphology and Processes. *Geografiska*
623 *Annaler. Series A, Physical Geography*, 49(1), 1. <https://doi.org/10.2307/520865>
- 624 Bates, C. C. (1953). Rational Theory of Delta Formation. *AAPG Bulletin*, 37.
625 <https://doi.org/10.1306/5CEADD76-16BB-11D7-8645000102C1865D>
- 626 Bentley, S. J., Blum, M. D., Maloney, J., Pond, L., & Paulsell, R. (2016). The Mississippi River source-to-
627 sink system: Perspectives on tectonic, climatic, and anthropogenic influences, Miocene to
628 Anthropocene. *Earth-Science Reviews*, 153, 139–174. <https://doi.org/10.1016/j.earscirev.2015.11.001>
- 629 Blair, T. C., & McPherson, J. G. (1994). Alluvial Fans and their Natural Distinction from Rivers Based on
630 Morphology, Hydraulic Processes, Sedimentary Processes, and Facies Assemblages. *SEPM Journal of*
631 *Sedimentary Research*, Vol. 64A. <https://doi.org/10.1306/D4267DDE-2B26-11D7-8648000102C1865D>
- 632 Blum, M. D., & Roberts, H. H. (2009). Drowning of the Mississippi Delta due to insufficient sediment
633 supply and global sea-level rise. *Nature Geoscience*, 2(7), 488–491. <https://doi.org/10.1038/ngeo553>
- 634 Bramble, M. S., Goudge, T. A., Milliken, R. E., & Mustard, J. F. (2019). Testing the deltaic origin of fan
635 deposits at Bradbury Crater, Mars. *Icarus*, 319, 363–366. <https://doi.org/10.1016/j.icarus.2018.09.024>
- 636 Broaddus, C. M., Vulis, L. M., Nienhuis, J. H., Tejedor, A., Brown, J., Foufoula-Georgiou, E., & Edmonds, D.
637 A. (2022). First-Order River Delta Morphology Is Explained by the Sediment Flux Balance From Rivers,
638 Waves, and Tides. *Geophysical Research Letters*, 49(22). <https://doi.org/10.1029/2022GL100355>
- 639 Brooke, S., Chadwick, A. J., Silvestre, J., Lamb, M. P., Edmonds, D. A., & Ganti, V. (2022). Where rivers
640 jump course. *Science*, 376(6596), 987–990. <https://doi.org/10.1126/science.abm1215>
- 641 Bryant, M., Falk, P., & Paola, C. (1995). Experimental study of avulsion frequency and rate of deposition.
642 *Geology*, 23(4), 365. [https://doi.org/10.1130/0091-7613\(1995\)023%253C0365:ESOAF%253E2.3.CO;2](https://doi.org/10.1130/0091-7613(1995)023%253C0365:ESOAF%253E2.3.CO;2)
- 643 Chakraborty, T., Kar, R., Ghosh, P., & Basu, S. (2010). Kosi megafan: Historical records, geomorphology
644 and the recent avulsion of the Kosi River. *Quaternary International*, 227(2), 143–160.
645 <https://doi.org/10.1016/j.quaint.2009.12.002>
- 646 Chamberlain, E. L., Törnqvist, T. E., Shen, Z., Mauz, B., & Wallinga, J. (2018). Anatomy of Mississippi Delta
647 growth and its implications for coastal restoration. *Science Advances*, 4(4), eaar4740.
648 <https://doi.org/10.1126/sciadv.aar4740>

649 Chatanantavet, P., & Lamb, M. P. (2014). Sediment transport and topographic evolution of a coupled
650 river and river plume system: An experimental and numerical study: EXPERIMENTS COUPLED RIVER &
651 RIVER-PLUME. *Journal of Geophysical Research: Earth Surface*, *119*(6), 1263–1282.
652 <https://doi.org/10.1002/2013JF002810>

653 Chatanantavet, P., Lamb, M. P., & Nittrouer, J. A. (2012). Backwater controls of avulsion location on
654 deltas. *Geophysical Research Letters*, *39*(1), 2011GL050197. <https://doi.org/10.1029/2011GL050197>

655 Chen, C., Tian, B., Schwarz, C., Zhang, C., Guo, L., Xu, F., Zhou, Y., & He, Q. (2021). Quantifying delta
656 channel network changes with Landsat time-series data. *Journal of Hydrology*, *600*, 126688.
657 <https://doi.org/10.1016/j.jhydrol.2021.126688>

658 Coffey, T. S., & Shaw, J. B. (2017). Congruent Bifurcation Angles in River Delta and Tributary Channel
659 Networks. *Geophysical Research Letters*, *44*(22). <https://doi.org/10.1002/2017GL074873>

660 Davidson, S. K., & Hartley, A. J. (2014). A Quantitative Approach To Linking Drainage Area and
661 Distributive-Fluvial-System Area In Modern and Ancient Endorheic Basins. *Journal of Sedimentary
662 Research*, *84*(11), 1005–1020. <https://doi.org/10.2110/jsr.2014.79>

663 Davidson, S. K., Hartley, A. J., Weissmann, G. S., Nichols, G. J., & Scuderi, L. A. (2013). Geomorphic
664 elements on modern distributive fluvial systems. *Geomorphology*, *180–181*, 82–95.
665 <https://doi.org/10.1016/j.geomorph.2012.09.008>

666 De Toffoli, B., Plesa, A. -C., Hauber, E., & Breuer, D. (2021). Delta Deposits on Mars: A Global Perspective.
667 *Geophysical Research Letters*, *48*(17), e2021GL094271. <https://doi.org/10.1029/2021GL094271>

668 Devauchelle, O., Petroff, A. P., Seybold, H. F., & Rothman, D. H. (2012). Ramification of stream networks.
669 *Proceedings of the National Academy of Sciences*, *109*(51), 20832–20836.
670 <https://doi.org/10.1073/pnas.1215218109>

671 Di Achille, G., & Hynes, B. M. (2010). Ancient ocean on Mars supported by global distribution of deltas
672 and valleys. *Nature Geoscience*, *3*(7), 459–463. <https://doi.org/10.1038/ngeo891>

673 Dong, T. Y., Nittrouer, J. A., Il'icheva, E., Pavlov, M., McElroy, B., Czapiga, M. J., Ma, H., & Parker, G.
674 (2016). Controls on gravel termination in seven distributary channels of the Selenga River Delta, Baikal
675 Rift basin, Russia. *Geological Society of America Bulletin*, *128*(7–8), 1297–1312.
676 <https://doi.org/10.1130/B31427.1>

677 Donselaar, M. E., Cuevas Gozalo, M. C., & Moyano, S. (2013). Avulsion processes at the terminus of low-
678 gradient semi-arid fluvial systems: Lessons from the Río Colorado, Altiplano endorheic basin, Bolivia.
679 *Sedimentary Geology*, *283*, 1–14. <https://doi.org/10.1016/j.sedgeo.2012.10.007>

680 Edmonds, D. A., Martin, H. K., Valenza, J. M., Henson, R., Weissmann, G. S., Miltenberger, K., Mans, W.,
681 Moore, J. R., Slingerland, R. L., Gibling, M. R., Bryk, A. B., & Hajek, E. A. (2022). Rivers in reverse:
682 Upstream-migrating dechannelization and flooding cause avulsions on fluvial fans. *Geology*, *50*(1), 37–
683 41. <https://doi.org/10.1130/G49318.1>

684 Edmonds, D. A., Paola, C., Hoyal, D. C. J. D., & Sheets, B. A. (2011). Quantitative metrics that describe
685 river deltas and their channel networks. *Journal of Geophysical Research*, *116*(F4), F04022.
686 <https://doi.org/10.1029/2010JF001955>

687 Edmonds, D. A., & Slingerland, R. L. (2007). Mechanics of river mouth bar formation: Implications for the
688 morphodynamics of delta distributary networks. *Journal of Geophysical Research: Earth Surface*,
689 *112*(F2), 2006JF000574. <https://doi.org/10.1029/2006JF000574>

690 ESRI. (2025). *World Imagery* [Imagery layer]. Esri, Maxar.
691 <https://www.arcgis.com/home/item.html?id=10df2279f9684e4a9f6a7f08febac2a9>

692 Fagherazzi, S. (2008). Self-organization of tidal deltas. *Proceedings of the National Academy of Sciences*,
693 *105*(48), 18692–18695. <https://doi.org/10.1073/pnas.0806668105>

694 Fagherazzi, S., Edmonds, D. A., Nardin, W., Leonardi, N., Canestrelli, A., Falcini, F., Jerolmack, D. J.,
695 Mariotti, G., Rowland, J. C., & Slingerland, R. L. (2015). Dynamics of river mouth deposits. *Reviews of*
696 *Geophysics*, *53*(3), 642–672. <https://doi.org/10.1002/2014RG000451>

697 Farley, K. A., Williford, K. H., Stack, K. M., Bhartia, R., Chen, A., De La Torre, M., Hand, K., Goreva, Y.,
698 Herd, C. D. K., Hueso, R., Liu, Y., Maki, J. N., Martinez, G., Moeller, R. C., Nelessen, A., Newman, C. E.,
699 Nunes, D., Ponce, A., Spanovich, N., ... Wiens, R. C. (2020). Mars 2020 Mission Overview. *Space Science*
700 *Reviews*, *216*(8), 142. <https://doi.org/10.1007/s11214-020-00762-y>

701 Federici, B., & Paola, C. (2003). Dynamics of channel bifurcations in noncohesive sediments. *Water*
702 *Resources Research*, *39*(6), 2002WR001434. <https://doi.org/10.1029/2002WR001434>

703 Fielding, C. R., Ashworth, P. J., Best, J. L., Prokocki, E. W., & Smith, G. H. S. (2012). Tributary, distributary
704 and other fluvial patterns: What really represents the norm in the continental rock record? *Sedimentary*
705 *Geology*, *261–262*, 15–32. <https://doi.org/10.1016/j.sedgeo.2012.03.004>

706 Fontana, A., Mozzi, P., & Marchetti, M. (2014). Alluvial fans and megafans along the southern side of the
707 Alps. *Sedimentary Geology*, *301*, 150–171. <https://doi.org/10.1016/j.sedgeo.2013.09.003>

708 Friend, P. F. (1978). *DISTINCTIVE FEATURES OF SOME ANCIENT RIVER SYSTEMS*.

709 Galloway, E. (1975). Process Framework for Describing the Morphologic and Stratigraphic Evolution of
710 Deltaic Depositional Systems. *Deltas: Models for Exploration, 1975*, 87–98.

711 Ganti, V., Chu, Z., Lamb, M. P., Nittrouer, J. A., & Parker, G. (2014). Testing morphodynamic controls on
712 the location and frequency of river avulsions on fans versus deltas: Huanghe (Yellow River), China.
713 *Geophysical Research Letters*, *41*(22), 7882–7890. <https://doi.org/10.1002/2014GL061918>

714 Gearon, J. H., Martin, H. K., DeLisle, C., Barefoot, E. A., Mohrig, D., Paola, C., & Edmonds, D. A. (2024).
715 Rules of river avulsion change downstream. *Nature*, *634*(8032), 91–95. <https://doi.org/10.1038/s41586-024-07964-2>

717 Geleynse, N., Storms, J. E. A., Walstra, D.-J. R., Jagers, H. R. A., Wang, Z. B., & Stive, M. J. F. (2011).
718 Controls on river delta formation; insights from numerical modelling. *Earth and Planetary Science*
719 *Letters*, *302*(1–2), 217–226. <https://doi.org/10.1016/j.epsl.2010.12.013>

720 Giosan, L., Syvitski, J., Constantinescu, S., & Day, J. (2014). Climate change: Protect the world's deltas.
721 *Nature*, *516*(7529), 31–33. <https://doi.org/10.1038/516031a>

722 Hansford, M. R., & Plink-Björklund, P. (2020). River discharge variability as the link between climate and
723 fluvial fan formation. *Geology*, *48*(10), 952–956. <https://doi.org/10.1130/G47471.1>

724 Hariharan, J., Piliouras, A., Schwenk, J., & Passalacqua, P. (2022). Width-Based Discharge Partitioning in
725 Distributary Networks: How Right We Are. *Geophysical Research Letters*, *49*(14), e2022GL097897.
726 <https://doi.org/10.1029/2022GL097897>

727 Harris, C. R., Millman, K. J., van der Walt, S. J., Gommers, R., Virtanen, P., Cournapeau, D., Wieser, E.,
728 Taylor, J., Berg, S., Smith, N. J., Kern, R., Picus, M., Hoyer, S., van Kerkwijk, M. H., Brett, M., Haldane, A.,
729 del Río, J. F., Wiebe, M., Peterson, P., ... Oliphant, T. E. (2020). Array programming with NumPy. *Nature*,
730 *585*(7825), 357–362. <https://doi.org/10.1038/s41586-020-2649-2>

731 Hartley, A. J., Weissmann, G. S., Nichols, G. J., & Warwick, G. L. (2010). Large Distributive Fluvial Systems:
732 Characteristics, Distribution, and Controls on Development. *Journal of Sedimentary Research*, *80*(2),
733 167–183. <https://doi.org/10.2110/jsr.2010.016>

734 Horton, B. K., & Decelles, P. G. (2001). *Modern and ancient Fluvial megafans in the foreland basin system*
735 *of the central Andes, southern Bolivia: Implications for drainage network evolution in fold-thrust belts*
736 (pp. 43–63).

737 Hunter, J. D. (2007). MATPLOTLIB - 2D GRAPHICS ENVIRONMENT. *Computing in Science & Engineering*.

738 Isikdogan, F., Bovik, A., & Passalacqua, P. (2017). RivaMap: An automated river analysis and mapping
739 engine. *Remote Sensing of Environment*, *202*, 88–97. <https://doi.org/10.1016/j.rse.2017.03.044>

740 Jerolmack, D. J. (2009). Conceptual framework for assessing the response of delta channel networks to
741 Holocene sea level rise. *Quaternary Science Reviews*, *28*(17–18), 1786–1800.
742 <https://doi.org/10.1016/j.quascirev.2009.02.015>

743 Jerolmack, D. J., & Swenson, J. B. (2007). Scaling relationships and evolution of distributary networks on
744 wave-influenced deltas. *Geophysical Research Letters*, *34*(23), 2007GL031823.
745 <https://doi.org/10.1029/2007GL031823>

746 Jones, L. S., & Schumm, S. A. (1999). Causes of Avulsion: An Overview. In N. D. Smith & J. Rogers (Eds.),
747 *Fluvial Sedimentology VI* (1st ed., pp. 169–178). Wiley. <https://doi.org/10.1002/9781444304213.ch13>

748 Ke, W., Shaw, J. B., Mahon, R. C., & Cathcart, C. A. (2019). Distributary Channel Networks as Moving
749 Boundaries: Causes and Morphodynamic Effects. *Journal of Geophysical Research: Earth Surface*, *124*(7),
750 1878–1898. <https://doi.org/10.1029/2019JF005084>

751 Kelly, S. B., & Olsen, H. (1993). Terminal fans a review with reference to Devonian examples. In
752 *Sedimentary Geology* (Vol. 85, pp. 339–374).

753 Lauzon, R., Piliouras, A., & Rowland, J. C. (2019). Ice and Permafrost Effects on Delta Morphology and
754 Channel Dynamics. *Geophysical Research Letters*, *46*(12), 6574–6582.
755 <https://doi.org/10.1029/2019GL082792>

756 Leier, A. L., DeCelles, P. G., & Pelletier, J. D. (2005). Mountains, monsoons, and megafans. *Geology*,
757 *33*(4), 289. <https://doi.org/10.1130/G21228.1>

758 Leonardi, N., Canestrelli, A., Sun, T., & Fagherazzi, S. (2013). Effect of tides on mouth bar morphology
759 and hydrodynamics. *Journal of Geophysical Research: Oceans*, *118*(9), 4169–4183.
760 <https://doi.org/10.1002/jgrc.20302>

761 Limaye, A. B., Adler, J. B., Moodie, A. J., Whipple, K. X., & Howard, A. D. (2023). Effect of Standing Water
762 on Formation of Fan-Shaped Sedimentary Deposits at Hypanis Valles, Mars. *Geophysical Research*
763 *Letters*, 50(4), e2022GL102367. <https://doi.org/10.1029/2022GL102367>

764 Mahon, R., Hughes, C., Chen, H., & Shaw, J. (2024). Ancient Channel-Mouth Bifurcation Angles on Earth
765 and Mars. *The Sedimentary Record*, 22(1). <https://doi.org/10.2110/001c.124824>

766 Malin, M. C., & Edgett, K. S. (2015). *Evidence for Persistent Flow and Aqueous Sedimentation on Early*
767 *Mars*. www.sciencemag.org

768 Martin, H. K., & Edmonds, D. A. (2023). Avulsion dynamics determine fluvial fan morphology in a cellular
769 model. *Geology*, 51(8), 796–800. <https://doi.org/10.1130/G51138.1>

770 Mendenhall, W., Beaver, R. J., & Beaver, B. M. (2012). *Introduction to Probability and Statistics*.
771 Brooks/Cole.

772 Mohrig, D., Heller, P. L., Paola, C., & Lyons, W. J. (2000). Interpreting avulsion process from ancient
773 alluvial sequences: Guadalope-Matarranya system (northern Spain) and Wasatch Formation (western
774 Colorado). *Geological Society of America Bulletin*.

775 Morais, E. S., & Montanher, O. C. (2022). Avulsion in a meandering river: Floodplain conditions for
776 occurrence and effects in the parent channel. *CATENA*, 214, 106236.
777 <https://doi.org/10.1016/j.catena.2022.106236>

778 Morón, S., Amos, K., Edmonds, D. A., Payenberg, T., Sun, X., & Thyer, M. (2017). Avulsion triggering by El
779 Niño–Southern Oscillation and tectonic forcing: The case of the tropical Magdalena River, Colombia. *GSA*
780 *Bulletin*, 129(9–10), 1300–1313. <https://doi.org/10.1130/B31580.1>

781 Moscariello, A. (2018). Alluvial fans and fluvial fans at the margins of continental sedimentary basins:
782 Geomorphic and sedimentological distinction for geo-energy exploration and development. *Geological*
783 *Society, London, Special Publications*, 440(1), 215–243. <https://doi.org/10.1144/SP440.11>

784 Nichols, G. J. (1987). *STRUCTURAL CONTROLS ON FLUVIAL DISTRIBUTARY SYSTEMS-THE LUNA SYSTEM,*
785 *NORTHERN SPAIN*.

786 Nichols, G. J., & Fisher, J. A. (2007). Processes, facies and architecture of fluvial distributary system
787 deposits. *Sedimentary Geology*, 195(1–2), 75–90. <https://doi.org/10.1016/j.sedgeo.2006.07.004>

788 Nienhuis, J. H., Ashton, A. D., Edmonds, D. A., Hoitink, A. J. F., Kettner, A. J., Rowland, J. C., & Törnqvist,
789 T. E. (2020). Global-scale human impact on delta morphology has led to net land area gain. *Nature*,
790 577(7791), 514–518. <https://doi.org/10.1038/s41586-019-1905-9>

791 Nienhuis, J. H., Ashton, A. D., & Giosan, L. (2015). What makes a delta wave-dominated? *Geology*, 43(6),
792 511–514. <https://doi.org/10.1130/G36518.1>

793 Nienhuis, J. H., Hoitink, A. J. F. T., & Törnqvist, T. E. (2018). Future Change to Tide-Influenced Deltas.
794 *Geophysical Research Letters*, 45(8), 3499–3507. <https://doi.org/10.1029/2018GL077638>

795 North, C. P., & Warwick, G. L. (2007). Fluvial Fans: Myths, Misconceptions, and the End of the Terminal-
796 Fan Model. *Journal of Sedimentary Research*, 77(9), 693–701. <https://doi.org/10.2110/jsr.2007.072>

797 Olariu, C., & Bhattacharya, J. P. (2006). Terminal distributary channels and delta front architecture of
798 river-dominated delta systems. *Journal of Sedimentary Research*, 76(2), 212–233.
799 <https://doi.org/10.2110/jsr.2006.026>

800 Ori, G. G., Marinangeli, L., & Baliva, A. (2000). Terraces and Gilbert-type deltas in crater lakes in Ismenius
801 Lacus and Memnonia (Mars). *Journal of Geophysical Research: Planets*, 105(E7), 17629–17641.
802 <https://doi.org/10.1029/1999JE001219>

803 Owen, A., Nichols, G. J., Hartley, A. J., Weissmann, G. S., & Scuderi, L. A. (2015). Quantification of a
804 Distributive Fluvial System: The Salt Wash DFS of the Morrison Formation, SW U.S.A. *Journal of*
805 *Sedimentary Research*, 85(5), 544–561. <https://doi.org/10.2110/jsr.2015.35>

806 Paniagua-Aroyave, J. F., & Nienhuis, J. H. (2024). The Quantified Galloway Ternary Diagram of Delta
807 Morphology. *Journal of Geophysical Research: Earth Surface*, 129(11), e2024JF007878.
808 <https://doi.org/10.1029/2024JF007878>

809 Paola, C., Twilley, R. R., Edmonds, D. A., Kim, W., Mohrig, D., Parker, G., Viparelli, E., & Voller, V. R.
810 (2011). Natural Processes in Delta Restoration: Application to the Mississippi Delta. *Annual Review of*
811 *Marine Science*, 3(1), 67–91. <https://doi.org/10.1146/annurev-marine-120709-142856>

812 Parker, G., Paola, C., Whipple, K. X., & Mohrig, D. (1998). ALLUVIAL FANS FORMED BY CHANNELIZED
813 FLUVIAL AND SHEET FLOW. I: THEORY. *Journal OF Hydraulic Engineering*, 985–995.

814 Passalacqua, P. (2017). The Delta Connectome: A network-based framework for studying connectivity in
815 river deltas. *Geomorphology*, 277, 50–62. <https://doi.org/10.1016/j.geomorph.2016.04.001>

816 Pearson, S. G., Van Prooijen, B. C., Elias, E. P. L., Vitousek, S., & Wang, Z. B. (2020). Sediment
817 Connectivity: A Framework for Analyzing Coastal Sediment Transport Pathways. *Journal of Geophysical*
818 *Research: Earth Surface*, 125(10), e2020JF005595. <https://doi.org/10.1029/2020JF005595>

819 Piliouras, A., Lauzon, R., & Rowland, J. C. (2021). Unraveling the Combined Effects of Ice and Permafrost
820 on Arctic Delta Morphodynamics. *Journal of Geophysical Research: Earth Surface*, 126(4),
821 e2020JF005706. <https://doi.org/10.1029/2020JF005706>

822 Pizzuto, J. E. (1987). Sediment diffusion during overbank flows. *Sedimentology*, 34(2), 301–317.
823 <https://doi.org/10.1111/j.1365-3091.1987.tb00779.x>

824 Plink-Björklund, P. (2021). Distributive Fluvial Systems: Fluvial and Alluvial Fans. In *Encyclopedia of*
825 *Geology* (pp. 745–758). Elsevier. <https://doi.org/10.1016/B978-0-08-102908-4.00015-1>

826 Radebaugh, J., Ventra, D., Lorenz, R. D., Farr, T., Kirk, R., Hayes, A., Malaska, M. J., Birch, S., Liu, Z. Y.-C.,
827 Lunine, J., Barnes, J., Le Gall, A., Lopes, R., Stofan, E., Wall, S., & Paillou, P. (2018). Alluvial and fluvial fans
828 on Saturn’s moon Titan reveal processes, materials and regional geology. *Geological Society, London,*
829 *Special Publications*, 440(1), 281–305. <https://doi.org/10.1144/SP440.6>

830 Rahman, M. M., Howell, J. A., & MacDonald, D. I. M. (2022). Quantitative analysis of crevasse-splay
831 systems from modern fluvial settings. *Journal of Sedimentary Research*, 92(9), 751–774.
832 <https://doi.org/10.2110/jsr.2020.067>

833 Reitz, M. D., & Jerolmack, D. J. (2012). Experimental alluvial fan evolution: Channel dynamics, slope
834 controls, and shoreline growth. *Journal of Geophysical Research: Earth Surface*, 117(F2), 2011JF002261.
835 <https://doi.org/10.1029/2011JF002261>

836 Saito, Y., Thanawat, J., Chaimanee, N., Jarupongsakul, T., & Syvitski, J. P. M. (2007). *Shrinking
837 Megadeltas in Asia: Sea-level Rise and Sediment Reduction Impacts from Case Study of the Chao Phraya
838 Delta The Holocene Red River Delta, Vietnam View project Global Risks and research priorities for coastal
839 subsidence View project Shrinking Megadeltas in Asia: Sea-level Rise and Sediment Reduction Impacts
840 from Case Study of the Chao Phraya Delta*. <https://www.researchgate.net/publication/234045413>

841 Schumm, S. A. (1977). The fluvial system. *Food and Agriculture Organization of the United Nations*.

842 Schwanghart, W., & Kuhn, N. J. (2010). TopoToolbox: A set of Matlab functions for topographic analysis.
843 *Environmental Modelling & Software*, 25(6), 770–781. <https://doi.org/10.1016/j.envsoft.2009.12.002>

844 Seybold, H., Andrade, J. S., & Herrmann, H. J. (2007). Modeling river delta formation. *Proceedings of the
845 National Academy of Sciences*, 104(43), 16804–16809. <https://doi.org/10.1073/pnas.0705265104>

846 Seybold, H. J., Kite, E., & Kirchner, J. W. (2018). Branching geometry of valley networks on Mars and
847 Earth and its implications for early Martian climate. *Science Advances*, 4(6), eaar6692.
848 <https://doi.org/10.1126/sciadv.aar6692>

849 Seybold, H., Rothman, D. H., & Kirchner, J. W. (2017). Climate’s watermark in the geometry of stream
850 networks. *Geophysical Research Letters*, 44(5), 2272–2280. <https://doi.org/10.1002/2016GL072089>

851 Shaw, J. B., Miller, K., & McElroy, B. (2018). Island Formation Resulting From Radially Symmetric Flow
852 Expansion. *Journal of Geophysical Research: Earth Surface*, 123(2), 363–383.
853 <https://doi.org/10.1002/2017JF004464>

854 Singh, H., Parkash, B., & Gohain, K. (1993). Facies analysis of the Kosi megafan deposits. *Sedimentary
855 Geology*, 85(1–4), 87–113. [https://doi.org/10.1016/0037-0738\(93\)90077-I](https://doi.org/10.1016/0037-0738(93)90077-I)

856 Sinha, R. (2009). The Great avulsion of Kosi on 18 August 2008. *Current Science*, 97(3), 429–433.

857 Slingerland, R., & Smith, N. D. (1998). Necessary conditions for a meandering-river avulsion. *Geology*,
858 26(5), 435. [https://doi.org/10.1130/0091-7613\(1998\)026%253C0435:NCFAMR%253E2.3.CO;2](https://doi.org/10.1130/0091-7613(1998)026%253C0435:NCFAMR%253E2.3.CO;2)

859 Slingerland, R., & Smith, N. D. (2004). RIVER AVULSIONS AND THEIR DEPOSITS. *Annual Review of Earth
860 and Planetary Sciences*, 32(1), 257–285. <https://doi.org/10.1146/annurev.earth.32.101802.120201>

861 Smart, J. S. (1971). *QUANTITATIVE PROPERTIES OF DELTA CHANNEL NETWORKS*.

862 Syvitski, J. P. M., & Brakenridge, G. R. (2013). Causation and avoidance of catastrophic flooding along the
863 Indus River, Pakistan. *GSA Today*, 23(1), 4–10. <https://doi.org/10.1130/GSATG165A.1>

864 Syvitski, J. P. M., Kettner, A. J., Overeem, I., Hutton, E. W. H., Hannon, M. T., Brakenridge, G. R., Day, J.,
865 Vörösmarty, C., Saito, Y., Giosan, L., & Nicholls, R. J. (2009). Sinking deltas due to human activities.
866 *Nature Geoscience*, 2(10), 681–686. <https://doi.org/10.1038/ngeo629>

867 Tebolt, M., & Goudge, T. A. (2022). Global investigation of martian sedimentary fan features: Using
868 stratigraphic analysis to study depositional environment. *Icarus*, 372, 114718.
869 <https://doi.org/10.1016/j.icarus.2021.114718>

870 Tejedor, A., Longjas, A., Edmonds, D. A., Zaliapin, I., Georgiou, T. T., Rinaldo, A., & Foufoula-Georgiou, E.
871 (2017). Entropy and optimality in river deltas. *Proceedings of the National Academy of Sciences*, 114(44),
872 11651–11656. <https://doi.org/10.1073/pnas.1708404114>

873 Tejedor, A., Longjas, A., Zaliapin, I., & Foufoula-Georgiou, E. (2015). Delta channel networks: 1. A graph-
874 theoretic approach for studying connectivity and steady state transport on deltaic surfaces. *Water*
875 *Resources Research*, 51(6), 3998–4018. <https://doi.org/10.1002/2014WR016577>

876 Törnqvist, T. E., & Bridge, J. S. (2002). Spatial variation of overbank aggradation rate and its influence on
877 avulsion frequency. *Sedimentology*, 49(5), 891–905. <https://doi.org/10.1046/j.1365-3091.2002.00478.x>

878 Trampush, S. M., & Hajek, E. A. (2017). Preserving proxy records in dynamic landscapes: Modeling and
879 examples from the Paleocene-Eocene Thermal Maximum. *Geology*, 45(11), 967–970.
880 <https://doi.org/10.1130/G39367.1>

881 Trauth, M. H. (2006). *MATLAB® Recipes for Earth Sciences*.

882 Ventra, D., & Clarke, L. E. (2018). Geology and geomorphology of alluvial and fluvial fans: Current
883 progress and research perspectives. *Geological Society, London, Special Publications*, 440(1), 1–21.
884 <https://doi.org/10.1144/SP440.16>

885 Virtanen, P., Gommers, R., Oliphant, T. E., Haberland, M., Reddy, T., Cournapeau, D., Burovski, E.,
886 Peterson, P., Weckesser, W., Bright, J., van der Walt, S. J., Brett, M., Wilson, J., Millman, K. J., Mayorov,
887 N., Nelson, A. R. J., Jones, E., Kern, R., Larson, E., ... Vázquez-Baeza, Y. (2020). SciPy 1.0: Fundamental
888 algorithms for scientific computing in Python. *Nature Methods*, 17(3), 261–272.
889 <https://doi.org/10.1038/s41592-019-0686-2>

890 Vulis, L., Tejedor, A., Ma, H., Nienhuis, J. H., Broaddus, C. M., Brown, J., Edmonds, D. A., Rowland, J. C., &
891 Foufoula-Georgiou, E. (2023). River Delta Morphotypes Emerge From Multiscale Characterization of
892 Shorelines. *Geophysical Research Letters*, 50(7), e2022GL102684.
893 <https://doi.org/10.1029/2022GL102684>

894 Walker, H. J. (1998). Arctic Deltas. *Journal of Coastal Research*, 14(3), 718–738.

895 Wall, S., Hayes, A., Bristow, C., Lorenz, R., Stofan, E., Lunine, J., Le Gall, A., Janssen, M., Lopes, R., Wye,
896 L., Soderblom, L., Paillou, P., Aharonson, O., Zebker, H., Farr, T., Mitri, G., Kirk, R., Mitchell, K.,
897 Notarnicola, C., ... Ventura, B. (2010). Active shoreline of Ontario Lacus, Titan: A morphological study of
898 the lake and its surroundings. *Geophysical Research Letters*, 37(5), 2009GL041821.
899 <https://doi.org/10.1029/2009GL041821>

900 Wang, J., & Plink-Björklund, P. (2019). Stratigraphic complexity in fluvial fans: Lower Eocene Green River
901 Formation, Uinta Basin, USA. *Basin Research*, 31(5), 892–919. <https://doi.org/10.1111/bre.12350>

902 Waskom, M. (2021). seaborn: Statistical data visualization. *Journal of Open Source Software*, 6(60), 3021.
903 <https://doi.org/10.21105/joss.03021>

904 Weissman, G. S., Hartley, A. J., Nichols, G. J., Scuderi, L. A., Olson, M., Buehler, H., & Banteah, R. (2010).
905 *Fluvial form in modern continental sedimentary basins: Distributive fluvial systems*.
906 <https://doi.org/10.1016/j.geo>

907 Weissmann, G. S., Hartley, A. J., Nichols, G. J., Scuderi, L. A., Olson, M., Buehler, H., & Banteah, R. (2010).
908 Fluvial form in modern continental sedimentary basins: Distributive fluvial systems. *Geology*, 38(1), 39–
909 42. <https://doi.org/10.1130/G30242.1>

910 Weissmann, G. S., Hartley, A. J., Scuderi, L. A., Nichols, G. J., Owen, A., Wright, S., Felicia, A. L., Holland,
911 F., & Anaya, F. M. L. (2015). Fluvial geomorphic elements in modern sedimentary basins and their
912 potential preservation in the rock record: A review. *Geomorphology*, 250, 187–219.
913 <https://doi.org/10.1016/j.geomorph.2015.09.005>

914 Witek, P. P., & Czechowski, L. (2015). Dynamical modelling of river deltas on Titan and Earth. *Planetary*
915 *and Space Science*, 105, 65–79. <https://doi.org/10.1016/j.pss.2014.11.005>

916 Wolinsky, M. A., Edmonds, D. A., Martin, J., & Paola, C. (2010). Delta allometry: Growth laws for river
917 deltas. *Geophysical Research Letters*, 37(21), 2010GL044592. <https://doi.org/10.1029/2010GL044592>

918 Wood, L. J. (2006). Quantitative geomorphology of the Mars Eberswalde delta. *Geological Society of*
919 *America Bulletin*, 118(5–6), 557–566. <https://doi.org/10.1130/B25822.1>

920 Wright, L. D. (1977). Sediment transport and deposition at river mouths: A synthesis. *Geological Society*
921 *of America Bulletin*, 88(6), 857. [https://doi.org/10.1130/0016-
922 7606\(1977\)88%253C857:STADAR%253E2.0.CO;2](https://doi.org/10.1130/0016-7606(1977)88%253C857:STADAR%253E2.0.CO;2)

923 Xu, Z., & Plink-Björklund, P. (2023). Quantifying Formative Processes in River- and Tide-Dominated
924 Deltas for Accurate Prediction of Future Change. *Geophysical Research Letters*, 50(20), e2023GL104434.
925 <https://doi.org/10.1029/2023GL104434>

926 Yang, H. (2020). Numerical investigation of avulsions in gravel-bed braided rivers. *Hydrological*
927 *Processes*, 34(17), 3702–3717. <https://doi.org/10.1002/hyp.13837>

928